Title:

Galectin-3 C-epitope, ANP, PPIA, and albumin function as drug-responsive panel biomarkers and therapeutic targets in aging and pressure overload-induced cardiac hypertrophy

Authors:

Puja Laxmanrao Shinde[a,c], Vikas Kumar [b,c,f,g], Siddhartha Singh[a, d,g], K.C.Sivakumar[e] and Rashmi Mishra,[a,c,d]*

Running Title: Therapeutic and diagnostic markers in cardiac hypertrophy

Affiliations:

a. Translational Mechanobiology Laboratory, Rajiv Gandhi Centre for Biotechnology (RGCB), Thycaud PO, Poojappura, Thiruvananthapuram-695014, India.

b. Cardiovascular Diseases and Diabetes Biology Laboratory, Rajiv Gandhi Center for Biotechnology (RGCB), Thiruvananthapuram-695014, Kerala. India.

c. Manipal Academy of Higher Education, Manipal-576104, Karnataka, India

d. Regional Centre for Biotechnology, Faridabad, Haryana 121001, India.

e. Distributed Information Sub-Centre, Rajiv Gandhi Centre for Biotechnology (RGCB), Thycaud PO, Poojappura, Thiruvananthapuram-695014, India.

f. Current Address: Department of Medicine, NYU Grossman School of Medicine, New York, NY-10016, USA (V.K)

g. These authors contributed equally to the work

*** Correspondence to:**
Rashmi Mishra, PhD, Translational Mechanobiology Laboratory, Rajiv Gandhi Centre for Biotechnology, Thycaud PO, Poojappura, Thiruvananthapuram-695014, Kerala, India. Email rashmimishra@rgcb.res.in

Abbreviations: **ACTN2** - Alpha-Actinin-2 protein; **ALB**– Albumin; **ANP** - Atrial Natriuretic Peptide; **ANXA2** - Annexin A2; **Asn**– Asparagine; **Arg**– Arginine; **AR** - Amalaki Rasayana; **αSMA** - Alpha smooth muscle actin; **BA-**Biological aged rats; **BAPTA** - 1,2(Bis-2-amino-5-methylphenoxy)ethane-N,N,N′,N′-tetraacetic acid tetrakis-acetoxymethyl) ester);**CAMK2A** - Calcium/Calmodulin-dependent protein kinase II; **CAMK2D** - Calcium/Calmodulin dependent protein kinase II delta; **CaN**–Calcineurin; **CAV1** - Caveolin-1; **CD44** - Cluster of Differentiation 44; **CD68** - Cluster of Differentiation 68; **CH** - Cardiac hypertrophy; **CRD** - Carbohydrate Recognition Domain; **cTNT** - Cardiac troponin T; **D-HCM** - Dilated Hypertrophic cardiomyopathy; **EGFP** - Enhanced Green Fluorescent Protein; **EGFR** - Epidermal Growth

Factor Receptor; **ELISA** - Enzyme-linked immunosorbent assay; **FDA** - Food and Drug Administration; **GA** - Gallic Acid; **GAL-1** - Galectin-1; **Gal3** – Galectin-3; **Gal-3N** - Cleaved fragment of Galectin-3 N-terminal (AA1 to AA113); **Gal-3C** - Cleaved fragment of Galectin-3 C-terminal (AA114 to AA250); **GAL3BP** – Galectin-3-Binding Protein; **GAL-9** - Galectin-9; **GATA4** - GATA Binding Protein 4; **HCM** - Hypertrophic cardiomyopathy; **HEK293** - Human Embryonic Kidney 293 cells,; **HMGB1** - High Mobility Group Box 1; **IP**–Immunoprecipitation; **LDHA** - Lactate dehydrogenase A; ; **LVEF** – Left Ventricular Ejection Fraction; **LVFS** - Left Ventricular Fractional Shortening **LVH** – Left Ventricular Hypertrophy **MYH7** - beta-Myosin Heavy Chain protein; **MEF2A** - Myocyte-specific Enhancer Factor 2A; **mut R186S** - Mutant EGFP agged Galectin 3 with mutation of carbohdrate recognition binding domain (CRD), **NASH** – Non alcoholic Steatohepatitis; **NFATC2** - Nuclear Factor of Activated T-cells-cytoplasmic-calcineurin-dependent 2; **OBSCN** –Obscurin; **PLA**-Proximity Ligation Assay (Duolink); **PO-CH** - Pressure Overloaded rats with left ventricular cardiac hypertrophy; **PPIA** - Peptidylprolyl isomerase A (Cyclophilin A; **PPID** - Peptidylprolyl isomerase D; **RhoA** - Ras homolog family member A; **ROCK1** - Rho-associated coiled-coil-containing protein kinase 1;**TMOD1** - Tropomodulin-1; **WGA** – Wheat Germ Agglutinin;**WT** - Wild Type..

HIGHLIGHTS

- Galectin-3 C-epitope, ANP, PPIA, and ALB are elevated in aging and pressure overload driven left ventricular hypertrophy
- Amalaki Rasayana (AR) and Gallic Acid (GA) reduce these markers in cardiac tissue and circulation.
- AR and GA inhibit Galectin-3 secretion and oligomeric binding to cardiomyocyte surfaces
- AR and GA regulation occurs via phosphorylation-dependent cytoplasmic Galectin-3 retention
- These markers serve as potential therapeutic targets and diagnostic biomarkers.

GRAPHICAL ABSTRACT:

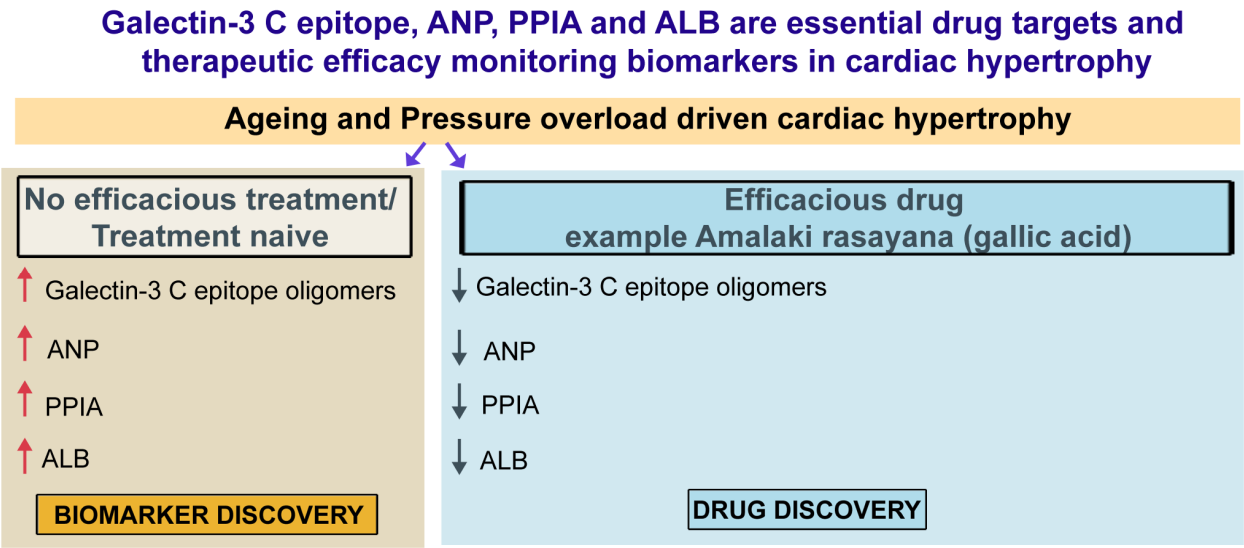

ABSTRACT:

Biological aging and pressure overload-induced left ventricular cardiac hypertrophy (PO-CH) is marked by myocardial thickening, fibrosis, and functional decline, heightening the risk of heart failure. To advance therapeutic monitoring and intervention, we aimed to identify drug-responsive biomarkers with functional relevance to disease progression. Using rat models of biological aging (BA) and PO-CH, we evaluated the cardioprotective effects of *Amalaki Rasayana* (AR), a traditional nutraceutical, and its bioactive constituent gallic acid (GA), while concurrently profiling candidate serum biomarkers. Galectin-3 was present in full-length and oligomeric forms, with C-terminal (C-epitope) homo-oligomers closely associated with pathological remodeling. AR and GA significantly reduced these oligomers via cytoplasmic retention and phosphorylation-dependent downregulation of galectin-3 secretion, mitigating maladaptive cardiomyocyte signaling. Levels of atrial natriuretic peptide (ANP), cyclophilin A (PPIA), and albumin (ALB) showed consistent changes, reinforcing their utility as therapeutic response indicators. Findings were validated in sera from aged humans and patients responsive to clinical treatment, confirming translational potential. This study establishes a novel biomarker panel-galectin-3 C-epitope, ANP, PPIA, and ALB-for monitoring treatment efficacy and positions AR as a promising intervention in cardiac hypertrophy.

KEYWORDS: Left ventricular cardiac hypertrophy (LV-HCM); dilated cardiac hypertrophy (D-HCM); biomarkers of drug therapy efficacy; pressure overload and cardiac hypertrophy, galectin-3 C epitope; Amalaki Rasayana; gallic acid

INTRODUCTION:

Hypertrophic cardiomyopathy (HCM), primarily driven by pressure overload in the left ventricle, and its advanced stage, dilated cardiomyopathy (D-HCM), represent major contributors to heart failure characterized by left ventricular systolic dysfunction and chamber dilatation [1, 2]. Initially, cardiomyocytes respond to elevated mechanical stress—arising from increased intraventricular pressure and a stiffened extracellular matrix—by hypertrophic growth, increasing in mass to maintain cardiac output [2]. However, chronic pressure overload eventually precipitates cardiomyocyte thinning, stretching, cellular damage, and death, culminating in D-HCM and progressive cardiac dysfunction [3]. Globally, the rising incidence of hospitalizations, readmissions, and mortality related to HCM and D-HCM highlights the urgent need for sensitive diagnostic and prognostic biomarkers that reflect disease progression and recovery [4, 5, 6].

Effective biomarkers should dynamically correlate with disease severity, increasing during exacerbation and declining with recovery, thereby serving not only as indicators but also as therapeutic targets. Importantly, biomarker-guided drug therapy enables clinicians to tailor treatment regimens—optimizing drug choice, dosage, and duration—and ultimately improving patient outcomes [5]. Such ideal biomarkers must possess high sensitivity, specificity, stability, cost-effectiveness, and minimal invasiveness, while maintaining reliability across diverse populations and sexes [6].

Myocardial fibrosis is a key pathological driver of hypertrophic and dilated cardiac failure. Fibrotic remodeling increases left ventricular stiffness, promotes ventricular dyssynchrony and tissue heterogeneity, and elevates cardiac afterload, thereby escalating the risk of heart failure and sudden cardiac death [5, 6]. Consequently, biomarkers and drug targets emerging from the cardiac fibrotic proteome hold considerable promise. Among these, galectin-3 (gal-3)—a beta-galactoside-binding lectin—has garnered attention due to its strong association with myocardial fibrosis, left ventricular dysfunction, and adverse cardiac outcomes [5, 6, 7]. Elevated circulating galectin-3 levels correlate with enhanced fibrosis, as gal-3 actively promotes fibroblast activation and scar formation in injured myocardium [8, 9]. The FDA's approval of galectin-3 assays for prognostic use in heart failure further validates its clinical utility in predicting mortality, hospitalization, and therapeutic response, with consistent performance across sexes and geographic regions [10, 11, 12].

Galectin-3 comprises two functional domains: an N-terminal domain (~110-115 amino acids, Gal-3N) and a C-terminal carbohydrate recognition domain (~130-150 amino acids, Gal-3C) [13]. This protein exists both as a full-length molecule (26–35 kDa) and in cleaved forms—Gal-3N (~15.5 kDa) and Gal-3C (~10.5 kDa)—likely generated extracellularly through proteolytic cleavage by collagenases and matrix metalloproteinases [13]. The C-terminal domain mediates glycan binding and oligomerization, facilitating significant signaling modulation and bioactivation [14, 15]. In cardiac tissue, galectin-3 C-terminal oligomers predominantly interact with glycosylated surface receptors on fibroblasts, macrophages, endothelial cells, and cardiomyocytes, linking galectin-3's molecular functions to crucial cellular processes in cardiac remodeling and disease [16]. We hypothesized that aberrant or elevated circulating levels of galectin-3 C-epitope oligomers could serve as superior biomarkers to inform therapeutic strategies in HCM and D-HCM.

Our objective was to demonstrate that therapeutic interventions targeting cardiac hypertrophy should focus on reducing the pool of galectin-3 C-epitope oligomers. By quantifying circulating gal-3C oligomers and monitoring their modulation during treatment, we aimed to correlate these levels with the progression or regression of hypertrophic cardiac damage. To test this, an in vivo drug model capable of alleviating left ventricular hypertrophy was essential to differentiate disease from recovery phases.

Amalaki rasayana (AR), a traditional Indian medicine derived from Phyllanthus emblica fruit, has gained recognition for its efficacy against biological and pathological cardiac hypertrophy [17, 18, 19]. Noted for its potent antioxidant, anti-fibrotic, and anti-aging properties, recent multi-omics studies have reinforced AR's role as a promising anti-cardiac hypertrophy agent [18, 19, 20]. AR is rich in gallic acid (GA) and its metabolite ellagic acid, both shown to confer cardioprotection via mechanisms including mitochondrial health enhancement [18, 21, 22]. Untargeted serum proteomics in AR-treated rat models have identified significant GA circulation, suggesting direct targeting of cardiac hypertrophy rather than mere metabolic byproducts like ellagic acid or urolithins [19]. Moreover, Bergenin—a natural GA derivative—has demonstrated in vitro inhibition of galectin-3 in cancer cell cultures, highlighting GA's therapeutic potential in regulating galectin-3 homeostasis [23, 24].

Using AR-based animal models of biological aging and pressure overload-induced pathological cardiac hypertrophy, we sought to elucidate the significance of galectin-3 C-epitope oligomers. We aimed to establish their superiority over full-length galectin-3 in evaluating drug efficacy against aging- and pressure overload-driven left ventricular hypertrophy. Our findings reveal a promising biomarker signature for monitoring cardiac hypertrophy treatment, detailed in the results section. Given the global burden of hypertrophic cardiac diseases, this research addresses a critical unmet need with the potential to transform therapeutic approaches for millions worldwide.

RESULTS:

Amalaki Rasayana (AR) significantly reduces extracellular and circulating galectin-3 C-epitope oligomers in a rat model of left ventricular cardiac hypertrophy (CH).

To evaluate the therapeutic potential of galectin-3 C-epitope as both a biomarker and drug target for cardiac hypertrophy (CH), we developed an in vivo Wistar rat model of CH induced by biological aging (BA) and pressure overload (PO). Recognizing the increasing interest in complementary and integrative medicine for cardiovascular health, we selected Amalaki Rasayana (AR), an Ayurvedic nutraceutical with established antioxidant, anti-inflammatory, and cardioprotective properties, as the intervention agent [17, 18].

Rats were administered AR orally at a dosage of 500 mg/kg body weight, following previously established protocols [18]. Over the 21-month experimental period, we assessed a comprehensive range of cardiac function parameters to determine AR's efficacy (see experimental design, **Figure 1A).** Compared with untreated BA and PO-CH controls, AR-treated cohorts exhibited significant improvement in echocardiographic indices, including left ventricular fractional shortening (LVFS) and ejection fraction (LVEF) **(Figure 1B–D)**.

Furthermore, AR-treated rats demonstrated superior physical performance, as evidenced by enhanced treadmill endurance **(Figure 1E)**. Histological analyses revealed a marked reduction in activated macrophages and fibroblasts—key contributors to myocardial fibrosis and calcification—in AR-treated hearts **(Figure 1F–M)**. This was accompanied by a notable decrease in fibrotic and calcified myocardial areas, along with better preservation of left ventricular wall structure and cardiomyocyte density **(Figure 2A, B)**.

282 Morphometric analysis of cardiomyocytes showed a significant reduction in cell surface area
283 in AR-treated rats, indicating attenuated myocyte hypertrophy **(Figure 2C–F)**. Additionally,
284 there was an increase in total myocardial cellular biomass, suggesting improved tissue
285 integrity and regenerative response **(Figure 2G–J)**. Biochemical assays revealed significantly
286 lower serum levels of lactate dehydrogenase-A (LDHA) and high mobility group box 1
287 (HMGB1), indicating improved membrane integrity and reduced cellular damage in AR-
288 treated rats **(Figure 2K, top panel)**.
289
290 Gene expression profiling further supported these findings. AR treatment was associated with
291 significant downregulation of fetal and hypertrophy-associated genes (ANP, GATA4, MYH7,
292 MEF2A, CAMK2D, CnNA, NFATC2) and upregulation of adult cardiac contractility
293 markers (cTNT, ACTN2, TMOD1, OBSCN, SERC2A), suggesting a shift towards a
294 physiologically mature myocardial phenotype **(Figure 2K, lower panels)**.
295
296 Given galectin-3's established role in promoting cardiac fibrosis, we hypothesized that AR
297 exerts its cardioprotective effects in part by suppressing galectin-3 signaling. Notably, long-
298 term AR administration (≥12 months) led to a significant decline in total serum oligomeric
299 galectin-3 levels **(Figure 3A–D)**, with a pronounced reduction in the C-terminal galectin-3
300 epitope oligomers—particularly relevant in both BA and PO-CH models **(Figure 3E–G)**.
301
302 Collectively, these results underscore the potential of AR as a promising therapeutic
303 intervention for cardiac hypertrophy, with the galectin-3 C-epitope emerging as a critical
304 molecular target. These findings warrant further investigation into galectin-3 C-epitope's
305 biomarker utility and translational relevance in human cardiac pathologies.
306
307 **The galectin-3 C-epitope oligomers play a dominant role in the generation of cardiac**
308 **hypertrophy.**
309
310 To elucidate the role of galectin-3 C-epitope oligomers in the pathogenesis of cardiac
311 hypertrophy, we employed a molecular strategy involving the expression of EGFP-tagged
312 full-length wild-type galectin-3 (Gal-3 WT-EGFP) and a carbohydrate recognition domain
313 mutant (Gal-3 R186S, hereafter referred to as CRD-MUT-Gal-3 EGFP), which is deficient in
314 binding β-galactoside-containing carbohydrate moieties [25]. HEK293 cells were used as a
315 heterologous overexpression system to ensure high transfection efficiency (~100%).

316 To simulate hypertrophic stress, we subjected one set of cells to pressure overload (PO) using
317 an established mechanical weight application method [26, 27], while another set served as an
318 untreated control (No PO). After 24 hours, conditioned media were collected from both Gal-3
319 WT-EGFP and CRD-MUT-Gal-3 EGFP expressing cells. Fluorescence intensities of the
320 secreted fusion proteins were measured using a multimode plate reader, and media were
321 normalized to equal fluorescence intensity to ensure consistent galectin-3 protein levels
322 across samples (2.5 mL per condition; see experimental schema, **Figure 4A**).
323
324 The fluorescence-normalized conditioned media were then applied to primary
325 cardiomyocytes for 10 hours, followed by cell fixation and morphometric analysis.
326 Quantification of cardiomyocyte surface area revealed significantly less hypertrophic
327 enlargement in cells treated with CRD-MUT-Gal-3 EGFP media compared to those exposed
328 to Gal-3 WT-EGFP, under both No PO and PO conditions **(Figure 4B, C)**. Fluorescence
329 imaging further indicated that the CRD-MUT-Gal-3 exhibited markedly reduced surface
330 binding, correlating with diminished hypertrophic response **(Figure 4D,F)**.
331
332 Notably, Gal-3 WT-EGFP derived from PO-conditioned media displayed a distinct micron-
333 sized clustered pattern on the cardiomyocyte surface. In contrast, CRD-MUT-Gal-3 EGFP
334 exhibited a more diffuse and uniform staining pattern, suggesting a key role of the C-epitope
335 in oligomerization and membrane clustering **(Figure 4D,E)**.
336
337 To examine whether Amalaki Rasayana (AR) modulates galectin-3 secretion and cell surface
338 binding to prevent hypertrophy, we subjected cardiomyocytes to 24-hour PO stress followed
339 by treatment with 100 µg/mL AR (dose determined from MTT viability and cell count
340 assays; **Figure 5A, B)** for an additional 24 hours. The supernatant (media) analysis revealed
341 significantly decreased levels of unbound galectin-3 C-epitope oligomers in AR-treated
342 groups under both No PO and PO conditions, compared to their respective untreated controls
343 **(Figure 5C, D)**. Similarly, surface-bound C-epitope signal intensity was markedly reduced
344 upon AR treatment **(Figure 5E, F)**.
345
346 Interestingly, Western blot analysis of cell lysates indicated increased intracellular retention
347 of galectin-3 in AR-treated groups **(Figure 5G, H)**, suggesting that AR impedes galectin-3
348 secretion, possibly by modulating intracellular trafficking or release pathways [28, 29].

349 These findings were further validated in an in vivo rat model. Cardiomyocytes from
350 hypertrophied left ventricles under biological ageing (BA) and pressure overload-induced
351 cardiac hypertrophy (PO-CH) exhibited high levels of membrane-bound C-epitope oligomers,
352 which were significantly reduced in their respective AR-treated counterparts **(Figure 5I–L)**.
353 Moreover, surface staining in PO-CH tissues revealed intense C-epitope clustering that
354 exceeded the N-epitope signal, supporting a dominant surface residency of C-terminal
355 galectin-3 oligomers in the hypertrophic state **(Figure 5J–L)**.
356
357 Finally, human cardiac hypertrophy (CH) tissue samples showed a similar pattern of co-
358 localized surface staining for both N- and C-epitopes, mirroring the trends observed in the rat
359 model and reinforcing the translational relevance of these findings **(Figure 6A, B)**.
360
361 **Enriched in gallic acid (GA), the AR extract effectively reduces excess extracellular**
362 **levels of Galectin-3 C-epitope oligomers.**
363
364 To identify bioactive constituents within Amalaki Rasayana (AR) responsible for the
365 observed reduction in extracellular galectin-3 C-epitope (Gal-3C) oligomers, we performed in
366 silico docking and molecular dynamics (MD) simulations with 18 phytocompounds
367 previously identified in AR [18]. Among them, three compounds displayed strong binding
368 affinities toward the Gal-3C domain, with gallic acid (GA) emerging as a prominent
369 candidate **(Figure 7A)**.
370
371 Given AR's enrichment in GA, we further investigated GA's role in modulating Gal-3C
372 oligomerization and glycan-binding properties. MD simulations revealed that GA binds to the
373 carbohydrate recognition domain (CRD) of Gal-3C via hydrogen bonding interactions with
374 key residues Arg144, Asn160, and Asn164 **(Figure 7B)**, suggesting a potential mechanism
375 for its modulatory action.
376
377 Functional assays in cardiomyocytes treated with 100 µM GA—an effective dose established
378 through MTT viability and cell count analyses **(Figure 7C, D)**—demonstrated a significant
379 reduction in extracellular Gal-3C oligomers across three compartments: conditioned media,
380 cell surface, and intracellular lysates **(Figure 7E–J)**. This pattern mirrored the effects seen
381 with AR, supporting GA as a major active constituent.
382

383 Cellular imaging further confirmed that Gal-3C epitope signals were more intense and
384 clustered than those of the N-terminal epitope in untreated cells. Upon treatment with GA or
385 AR, both signal intensity and clustering were significantly diminished in pressure overload
386 (PO) and control (No PO) conditions **(Figure 8A–C)**. These effects were comparable to those
387 observed with BAPTA-AM, a calcium chelator, suggesting that GA and AR may reduce
388 galectin-3 secretion by lowering intracellular calcium levels—an established trigger of
389 galectin-3 exocytosis [28].
390
391 To explore intracellular retention mechanisms, we performed in situ proximity ligation assays
392 (PLA), which demonstrated that GA enhances cytoplasmic retention of Gal-3, likely by
393 promoting serine phosphorylation at the S6 residue of the N-terminal domain—a
394 modification catalyzed by casein kinase 1 (CKI) **(Figure 8D, E)** [29, 30]. Consistent with
395 calcium regulation, BAPTA-AM also increased Gal-3 S6 phosphorylation and retention,
396 indicating that reduced cytosolic calcium facilitates CKI-mediated phosphorylation.
397
398 Supporting in vitro findings, left ventricular tissues from both biological ageing (BA) and
399 PO-induced hypertrophy (PO-CH) animal models showed significantly higher
400 phosphorylated Gal-3 levels in AR-treated cohorts **(Figure 8F, G)**. Furthermore, cardiac
401 tissues from hypertrophic cardiomyopathy (HCM) patients exhibited markedly lower Gal-3
402 phosphorylation than healthy donor hearts, consistent with excessive extracellular release and
403 decreased cytoplasmic retention in pathological states **(Figure 8H, I)**.
404
405 Immunoprecipitation (IP) of cardiomyocyte lysates with anti-Gal-3 antibody confirmed that
406 GA-treated cells retained a heavily phosphorylated intracellular Gal-3 pool compared to
407 untreated controls **(Figure 8J, K)**. To dissect the specificity of GA-mediated
408 phosphorylation, we engineered Gal-3 CRD mutants lacking GA-binding sites and
409 overexpressed these constructs in cardiomyocytes. Upon exposure to PO ± GA, cells
410 expressing triple CRD mutants displayed significantly lower S6 phosphorylation compared to
411 wild-type Gal-3 **(Figure 8L, M)**, demonstrating that GA binding is necessary for
412 phosphorylation.
413
414 Additionally, cells expressing the S6A Gal-3 mutant, incapable of being phosphorylated at
415 the N-epitope, showed no increase in phosphorylation upon GA treatment, confirming that
416 CKI-mediated S6 phosphorylation is a key regulatory mechanism **(Figure 8L, M)**. IP using

417 N-epitope GFP-tagged Gal-3 ± GA validated GA's role in enhancing N-epitope
418 phosphorylation, whereas IP with C-epitope-tagged constructs showed no significant change,
419 indicating specificity of GA-induced modifications to the N-terminal region **(Figure 8L, M)**.
420 To assess the likely impact of GA on galectin-3 glycan-binding, we pre-mixed PO-
421 conditioned media from WT Gal-3-GFP-expressing cardiomyocytes with lactose before
422 incubation on fresh cardiomyocytes. Surface fluorescence analysis revealed significantly
423 reduced Gal-3 binding in a lactose dependent manner **(Figure 8N–P)**, suggesting that GA
424 interferes with glycan interactions of Gal-3, likely via its CRD, akin to lactose.
425
426 Collectively, these data suggest that GA acts through dual mechanisms: (1) by chelating
427 cytosolic calcium, thus reducing secretion of Gal-3C oligomers, and (2) by binding to the
428 Gal-3 CRD, inducing conformational changes that expose the S6 site for CKI-mediated
429 phosphorylation. This dual action promotes intracellular retention and reduces surface
430 clustering of galectin-3, thereby mitigating its hypertrophic effects.
431
432 Indeed, literature supports this mechanistic framework. Elevated cytosolic calcium—common
433 under mechanical stress or pressure overload—activates calcineurin A, a phosphatase that
434 antagonizes CKI activity, thereby reducing galectin-3 phosphorylation and enhancing its
435 secretion [31, 32]. Our findings suggest that GA, by modulating both calcium signaling and
436 phosphorylation, shifts galectin-3 toward a non-pathogenic intracellular fate, offering a
437 promising therapeutic strategy.
438
439 Ongoing studies aim to further delineate the structural basis by which GA and AR influence
440 galectin-3 conformations, phosphorylation dynamics, and calcium homeostasis in cardiac
441 hypertrophy.
442
443 **Sera and tissue samples from human donors confirm the pivotal role of the galectin-3**
444 **C-epitope in the generation of cardiac hypertrophy (CH).**
445
446 During cardiac hypertrophy (CH), the plasma membrane of cardiomyocytes experiences
447 dynamic changes due to hydrostatic pressure. As depicted in the schematic **(Figure 12),** this
448 mechanical load and accompanying membrane stretch are sensed by surface mechanosensors,
449 which activate the RhoA-ROCK signaling pathway to stabilize F-actin stress fibers that help
450 resist the mechanical strain [33]. Literature and our findings together suggest that during

transient pressure, F-actin stress fibers serve a protective role; however, to accommodate extended fiber length, hypertrophy-associated genes are upregulated, leading to increased cardiomyocyte surface area.

Under sustained mechanical load, however, the RhoA-ROCK1 axis and extensive stress fiber formation lead to maladaptive signaling. RhoA-induced cytoplasmic calcium elevation triggers aberrant activation of hypertrophy-associated genes such as NFATC2, MEF2A, and GATA4 [33, 34]. Rigid, bundled F-actin stress fibers deform the nucleus, affecting chromatin stability, and simultaneously cause disassembly of caveolae—the principal mechanoprotective membrane invaginations—by removing the caveolar protein PTRF. This leads to heightened membrane tension [35].

Elevated cytosolic calcium also promotes the over-secretion of galectin-3 [28]. The secreted galectin-3 binds and activates membrane receptors such as EGFR, CD44, and integrins, initiating their autophosphorylation [36, 37, 38, 39]. This further amplifies deleterious RhoA-ROCK1 signaling and activates cSrc kinase, which phosphorylates CAV1, a structural caveolae protein, resulting in additional caveolar loss [40, 41]. This cascade accelerates CH progression, increases membrane permeability, and contributes to cardiomyocyte loss. Excess circulating galectin-3 may also act systemically, leading to dysfunction in peripheral tissues.

To evaluate the clinical relevance of galectin-3 C-epitope in human hypertrophic cardiomyopathy (HCM), we analyzed serum samples from young and old healthy donors and HCM survivors undergoing treatment. Atrial natriuretic peptide (ANP), secreted by cardiomyocytes in response to mechanical stress, served as a tension biomarker **(Figure 9A, B)**. Older individuals and HCM patients had elevated ANP levels compared to younger donors, reflecting increased myocardial wall stress. Notably, ANP levels in HCM patients were comparable to aged healthy controls, suggesting therapeutic benefit from clinical interventions.

We next analyzed serum galectin-3 C-epitope oligomers via Western blotting **(Figure 9C, D)**. HCM survivors exhibited slightly lower C-epitope oligomer levels than aged healthy controls, implying reduced cardiac strain due to treatment. Young donors with low ANP also showed lower C-epitope levels. Interestingly, ELISA analysis for total galectin-3 did not correlate with the oligomer profile; HCM survivors showed the highest total galectin-3 levels

among all groups **(Figure 9E)**. This discrepancy underscores the limitations of ELISAs using full-length galectin-3 antibodies, which may not adequately detect C-epitope oligomers, thereby obscuring galectin-3's potential as a biomarker of treatment response in CH.

Although drug-naïve HCM patient sera were unavailable, our tissue analysis has revealed significantly higher C-epitope oligomer accumulation on cardiomyocyte surfaces in HCM drug-naïve hearts compared to age-matched controls **(Figure 6)**. Thus, reduced serum C-epitope levels in treated HCM patients likely reflect therapeutic efficacy, highlighting the utility of C-epitope oligomers as a treatment response biomarker.

Given that serum reflects tissue-level metabolic and secretory states, we investigated how donor sera affected cardiomyocyte hypertrophy. Cardiomyocytes incubated with sera from older donors exhibited increased cell surface area compared to those treated with sera from HCM patients on medication, mirroring the C-epitope oligomer profiles **(Figure 10A, B)**. To directly assess the role of the C-epitope, we enriched aged donor serum fractions for N- and C-epitopes via immunoprecipitation. Cardiomyocytes exposed to C-epitope-enriched fractions displayed significantly more hypertrophy than those treated with N-epitope-enriched fractions **(Figure 10C, D)**. Pre-incubation of the C-epitope fraction with lactose—a glycan-binding blocker—significantly attenuated this hypertrophy **(Figure 10C, D)**.

Furthermore, the surface clustering of C-epitope oligomers was markedly higher than that of N-epitopes, unless blocked by lactose **(Figure 10E, F)**. These results suggest that the galectin-3 C-epitope induces hypertrophy through its carbohydrate recognition domain (CRD), which facilitates oligomer binding to cell surfaces and activates mechanotransductive stress pathways.

Treatment of cardiomyocytes with gallic acid (GA) mimicked and exceeded the inhibitory effects of lactose on C-epitope-induced hypertrophy and surface oligomerization **(Figure 11A–D)**. In comparison to the N-epitope, C-epitope administration also elevated RhoA and ROCK1 expression **(Figure 11E–G)** [33, 34], enhanced F-actin stress fiber formation **(Figure 11C)** [42], promoted caveolae disassembly **(Figure 11H, I)** [40, 41], and increased cellular tension (increase in nuclear YAP1**, Figure 11J, K)** [43]. It also elevated nuclear envelope tension (increase in nuclear Lamin A, **Figure 11L, M**) [44], induced DNA damage **(Figure 11N, O)**, and upregulated hypertrophic gene expression **(Figure 11P–S)** [33].

519 Additionally, increased membrane permeability and cell loss were observed **(Figure 11T, U)**.
520 These pathological effects were significantly mitigated by lactose and GA, both of which
521 block the CRD of galectin-3.
522
523 Taken together, these findings underscore the essential role of the galectin-3 C-epitope CRD
524 in mediating cardiomyocyte hypertrophy and suggest that its inhibition by small molecules
525 such as GA may serve as a promising therapeutic approach. A graphical summary of these
526 results demonstrates the role of excessive galectin-3 C-epitope oligomers as critical drug
527 targets in cardiac hypertrophy **(Figure 12)**.
528
529 **Galectin-3 C-epitope, ANP, PPIA, and ALB are promising proteins for a biomarker**
530 **panel aimed at evaluating drug efficacy.**
531
532 Recognizing that galectin-3 is co-secreted with several proteins, we investigated their
533 potential inclusion in a multiplexed biomarker panel, alongside the galectin-3 C-epitope, to
534 improve the clinical assessment of drug response. Atrial natriuretic peptide (ANP) [45],
535 peptidyl-prolyl isomerases A ((PPIA)[46, 47], and albumin (ALB)[48, 49] are known to be
536 secreted into the serum either freely or encapsulated in extracellular vesicles such as
537 exosomes and microvesicles, in left ventricular hypertrophy.
538
539 Among these, ANP, PPIA, and ALB were prioritized based on their functional association
540 with cardiac pathology. We propose combining galectin-3 detection with natriuretic peptides
541 like ANP—secreted in abundance by mechanically stressed cardiomyocytes—to enhance
542 correlation between serum galectin-3 levels and cardiac tissue pathology **(Figure 9)**.
543 Additionally, PPIA and ALB are implicated in cardiovascular dysfunction and were found to
544 be dynamically regulated in our models.
545
546 In the pressure overload-induced cardiac hypertrophy (PO-CH) rat model, animals treated
547 with Amalaki Rasayana (AR) for at least 12 months showed a significant reduction in serum
548 levels of ANP, PPIA, ALB, and the galectin-3 C-epitope compared to untreated animals
549 **(Figure 13).** Similarly, aged (21-month-old) Wistar rats treated with AR also displayed lower
550 levels of these proteins than age-matched untreated controls, supporting the preventive
551 therapeutic efficacy of AR.
552

553 To evaluate the translational potential of this biomarker panel in humans, we conducted
554 Western blot analyses using serum samples from healthy donors and hypertrophic
555 cardiomyopathy (HCM) patients on drug therapy. Consistent with rodent findings, older
556 donors and HCM patients exhibited higher levels of ANP, PPIA, and ALB than younger
557 individuals **(Figure 9, 14)**. Importantly, the levels of ANP, PPIA, and ALB were comparable
558 between older healthy donors and treated HCM patients. However, C-epitope oligomer levels
559 were modestly lower in the HCM cohort than in healthy age-matched individuals, indicating
560 that C-epitope reduction could serve as a marker of treatment efficacy (Figure 9 and Figure
561 14).
562
563 Furthermore, donor samples exhibiting high levels of C-epitope oligomers also demonstrated
564 elevated concentrations of PPIA and ALB **(Figure 14)**, reinforcing the interrelationship
565 among these galectin-3-associated proteins. These findings support the inclusion of galectin-3
566 C-epitope, ANP, PPIA, and ALB in a multiplexed serum biomarker panel for the monitoring
567 of drug response and disease progression in CH.
568
569 Ongoing work is focused on quantifying the dynamic concentration ranges of these
570 biomarkers across larger and regionally diverse human cohorts. This data will be instrumental
571 in designing immunoassay and microfluidics-based biosensors for improving the predictive
572 accuracy and clinical utility of biomarker-based monitoring of drug efficacy in heart failure.
573
574 **DISCUSSION:**
575
576 In the context of aging-associated and pressure overload-induced left ventricular hypertrophy
577 (PO-CH/LVH), our findings present compelling evidence that the galectin-3 C-terminal
578 carbohydrate recognition domain (C-epitope) oligomers represent a more sensitive and
579 functionally relevant biomarker than full-length galectin-3 or its N-terminal counterparts.
580 Both in serum from aged human donors and in a pressure overload–cardiac hypertrophy (PO-
581 CH) animal model, we observed a significant increase in circulating C-epitope oligomers.
582 These changes correlated with elevated levels of atrial natriuretic peptide (ANP)—a known
583 marker of myocardial stretch—and other co-secreted proteins such as cyclophilin A (PPIA)
584 and albumin (ALB), suggesting a concerted secretory stress response associated with
585 myocardial remodeling [45-49].
586

587 Therapeutic intervention with Amalaki Rasayana (AR), an Ayurvedic polyherbal formulation
588 enriched in gallic acid, markedly reduced serum levels of galectin-3 C-epitope oligomers,
589 ANP, PPIA, and ALB. These reductions were associated with structural and functional
590 cardiac improvement in PO-CH models, positioning C-epitope oligomer profiling as a
591 reliable indicator of therapeutic efficacy. Our data support the concept that monitoring
592 galectin-3 C-epitope and its co-secreted partners can serve not only to gauge clinical recovery
593 in heart failure patients, but also to stratify risk and monitor prophylactic responses,
594 particularly in aging populations predisposed to cardiac stress [50, 51].
595
596 Mechanistically, AR appears to exert its cardioprotective effects in part through gallic acid's
597 high-affinity binding to the C-epitope CRD. This interaction competitively inhibits galectin-
598 3's glycan-dependent surface binding, thereby blocking downstream hypertrophic
599 mechanotransduction via RhoA-ROCK1 signaling and stress fiber formation. Moreover,
600 CRD binding by gallic acid facilitates conformational changes that expose galectin-3 to
601 phosphorylation, promoting its cytoplasmic retention and reducing extracellular secretion—
602 key steps in mitigating maladaptive cardiac remodeling [16, 33].
603
604 Importantly, serum analyses from hypertrophic cardiomyopathy (HCM) patients receiving
605 pharmacological treatment revealed lower levels of galectin-3 C-epitope oligomers compared
606 to age-matched healthy donors, despite having higher total galectin-3 levels. This uncoupling
607 of total and functional galectin-3 levels underscores the inadequacy of conventional full-
608 length galectin-3 ELISA platforms in accurately reflecting therapeutic impact. Our data show
609 that C-epitope levels, along with PPIA, ALB, and ANP, form a synergistic network that
610 better reflects disease progression and resolution than individual biomarkers alone.
611
612 These findings advocate for broader adoption of a multiplex biomarker panel, incorporating
613 galectin-3 C-epitope, PPIA, ALB, and ANP, to improve clinical stratification, prognosis, and
614 therapy response assessment in heart failure. We propose the development of low-cost, paper-
615 based multiplex diagnostic tools, high-sensitivity ELISA assays, and reverse-phase protein
616 array (RPPA) chips specifically designed to detect these markers in diverse patient
617 populations. Furthermore, clinical validation of AR's efficacy across large, geographically
618 distributed cohorts is urgently needed to establish its safety and translational potential in
619 cardiometabolic health.
620

621 Beyond cardiac hypertrophy, elevated levels of galectin-3 and its C-epitope oligomers have
622 been implicated in a spectrum of diseases including malignancies, non-alcoholic
623 steatohepatitis (NASH), chronic kidney disease, obesity, hypertension, inflammatory bowel
624 disease, dementia, diabetes, and even COVID-19[52-53]. Our study suggests that quantifying
625 galectin-3 C-epitope enrichment may offer a sensitive, functionally relevant window into
626 systemic disease states and therapeutic trajectories, offering promise for precision medicine
627 approaches in both cardiovascular and multisystem disorders.
628
629 **CONCLUSIONS:**
630
631 Galectin-3 performs multiple vital physiological functions, and thus, complete inhibition or
632 dysregulation of its endogenous and exogenous levels risks significant adverse effects [13,
633 16]. Our research distinctly highlights the pivotal role of galectin-3 C-epitope oligomeric
634 forms as superior, highly specific biomarker for the diagnosis and therapeutic monitoring of
635 hypertrophic cardiomyopathy, surpassing the diagnostic value of full-length galectin-3
636 protein.
637
638 These findings underscore the urgent need for the development of accessible, low-cost,
639 paper-based biomarker assays incorporating galectin-3 C-epitope in combination with PPIA,
640 ALB, and ANP, enabling sensitive and reliable clinical evaluation of cardiac hypertrophy and
641 drug efficacy.
642
643 Moreover, our work identifies the excessively secreted galectin-3 C-epitope oligomers as a
644 promising and actionable drug target in age-associated and pathological cardiac hypertrophy,
645 with Amalaki Rasayana demonstrating significant therapeutic potential to suppress these
646 harmful oligomeric pools and ameliorate cardiac remodeling (**Figure 15**).
647
648 Collectively, these insights pave the way for geroprotective and precision cardiovascular
649 medicine approaches focused on refined biomarker panels and targeted therapeutics to
650 mitigate cardiac hypertrophy and improve patient outcomes.
651
652
653
654

655 **MATERIALS AND METHODS:**

656

657 ***Reagents, Cell Lines, and Patient Samples***

658 Cell lines H9c2(2-1), HEK-293 (293), and CRL-1446 were procured from ATCC, Sigma, or
659 Lonza, unless otherwise stated. The pEGFP-hGal3 plasmid (#73080) was obtained from
660 Addgene (USA); other constructs were custom-synthesized by Zellebiotech.com. Most
661 reagents were purchased from Merck/Sigma-Aldrich. Galectin-3 ELISA kits—Rat
662 ERLGALS3 and Human DGAL30—were sourced from Thermo Scientific and R&D
663 Systems, respectively. Antibodies and dilutions used are as follows:CBP-112 AP, Rabbit
664 anti-Galectin-3 (C-epitope): 1:1000;CBP-101 AP, Rabbit anti-Galectin-3 (N-epitope):
665 1:1000;Galectin-3 Mouse mAb (B2C10, sc-32790): 1:500; A13506, Galectin-3 KO validated
666 ab 1:1000; NPPA Rabbit pAb (A1609): 1:5000; Albumin Rabbit pAb (A1363): 1:1000;Anti-
667 Cyclophilin A (PPIA, AB58144): 1:5000.Human heart tissue arrays were acquired from
668 Tissuearray.com (USA). Human serum samples were sourced from Innovative Research
669 (USA) following approval from the Institutional Human Ethics Committee of RGCB (File
670 no. IHEC/12/2023_Ex/07) and in accordance with ICMR guidelines, Government of India.

671

672 ***Development of a Drug Model for Cardiac Hypertrophy***

673 To validate a biomarker panel for assessing therapeutic efficacy in hypertrophic
674 cardiomyopathy (CH), a preclinical drug model with established anti-hypertrophic effects
675 was employed [18]. All animal procedures were approved by the Institutional Animal Ethics
676 Committee (IAEC) of RGCB and conducted in accordance with guidelines of the Committee
677 for Control and Supervision of Experiments on Animals (CCSEA), Government of India.
678 Three-month-old male Wistar rats (180–200 g) were housed under standard conditions (12 h
679 light/dark cycle, controlled temperature and humidity) with ad libitum access to synthetic
680 chow and water. Cardiac hypertrophy was induced by transverse aortic constriction (TAC)
681 using a titanium clip to reduce aortic diameter by ~60%. Anesthesia was administered using
682 3% isoflurane in 100% oxygen. Aortic constriction was verified via trans-thoracic 2D color
683 Doppler imaging. Sham-operated controls (BA and BA+AR) underwent identical surgery
684 without clip placement. Left ventricular hypertrophy was monitored from nine months of age.

685

686 *Two experimental arms were included:*

687 1. *Aging Group:* Sixteen rats were divided into 'BA' (biologically aged, sham control)
688 and 'BA+AR' groups. The BA+AR group received Amalaki Rasayana (AR) orally (500

689 mg/kg, 5 days/week) starting at 9 months, continued until 21 months. Dose selection was
690 based on prior efficacy and traditional use.
691 2. *LVH Group:* Sixteen rats underwent TAC at 3 months. From 9 months, one cohort
692 received AR ('PO-CH+AR'), while the other remained untreated ('PO-CH'). Treatment
693 continued until 21 months of age.
694 This model effectively simulates age-related and pressure overload-induced cardiac
695 hypertrophy for evaluating therapeutic interventions.
696
697 ***Drug Administration***
698 Amalaki Rasayana (AR) was prepared and characterized as previously described [18]. It was
699 administered orally each morning, 5 days per week, with a 2-day interval to allow systemic
700 clearance of excess components. In both the aging and pressure overload-induced cardiac
701 hypertrophy (PO-CH) groups, treatment continued until 21 months of age, ensuring at least
702 12 months of therapeutic exposure.
703
704 ***Echocardiography***
705 Echocardiographic evaluations were conducted at multiple time points before and during
706 treatment, up to 21 months of age, in both BA and PO-CH groups. Left ventricular
707 dimensions and ejection fraction were measured to assess the impact of AR on cardiac
708 changes associated with aging and pressure overload-induced hypertrophy.
709
710 ***Exercise Tolerance***
711 One month before study completion, all rats underwent a standardized treadmill protocol (30
712 min/day, 5 days/week). Tolerance was assessed by recording fatigue time and distance
713 covered at incremental speeds of 5, 10, and 15 m/min.
714
715 ***Tissue Collection***
716 At the end of the study, rats were euthanized, and cardiac tissues were collected. Samples
717 were either fixed in 10% neutral-buffered formalin for histology or stored in RNAlater for
718 downstream analyses, including Western blotting and qPCR. Formalin-fixed tissues were
719 processed for paraffin embedding.
720
721
722

723 ***Assessment of Cardiac Hypertrophy***

724 Cardiac fibrosis was assessed in 5 µm heart sections stained with Picrosirius Red (#365548,
725 Sigma). Slides were incubated in stain for 1 h, rinsed with distilled and acidified water,
726 dehydrated in graded ethanol and xylene, and mounted with DPX. Fibrotic area was
727 quantified using Fiji software and expressed as a percentage of total tissue area.
728 Cardiomyocyte hypertrophy was evaluated by measuring myocyte dimensions in Fiji
729 software.

730 Calcification was assessed using 1% Alizarin S (pH 4.2) staining. Sections were incubated
731 for 30 min at room temperature, rinsed, and then briefly immersed in acetone and an acetone–
732 xylene (1:1) mixture before clearing in xylene and mounting with DPX. Calcium deposits
733 appeared red to orange and were quantified using image analysis software.

734

735 ***Immunohistochemistry***

736 Slides were pre-baked at 55 °C for 15 min, de-paraffinized in xylene (2 × 20 min), and treated
737 with chloroform. Rehydration was performed through a graded ethanol series (100% to 70%,
738 5 min each). Sections were washed in PBS (pH 7.4) and permeabilized with 0.01% digitonin
739 in PBS for 30 min at room temperature.

740 Blocking was done using 3% BSA and 2% donkey serum in PBS for 1.5 h, followed by
741 overnight incubation with primary antibodies at 4 °C. After PBS washes, secondary
742 antibodies were applied for 1 h at room temperature. Nuclei were counterstained with DAPI
743 (5 min), and slides were mounted with 70% glycerol. Imaging and analysis followed
744 previously established protocols.

745

746 ***Cell Culture and Conditions***

747 Cardiomyoblasts were cultured in low-glucose DMEM supplemented with 10% FBS and
748 antibiotics (complete medium). For experiments, cells were seeded in 6-well plates, 8-well
749 chamber slides, or 96-well plates at densities of 0.1, 0.01, or 0.001 million cells/well,
750 respectively. After 24 h, differentiation into myocytes was induced by switching to serum-
751 reduced medium (DMEM with 1% FBS and antibiotics) for another 24 h. Cells were then
752 treated in complete medium containing 5% FBS.

753

754 ***MTT Assay for Dose Estimation of AR***

755 Cardiomyoblasts (5,000 cells/well) were seeded and differentiated in 96-well plates. Post-
756 differentiation, cells were treated with varying concentrations of AR (0, 5, 10, 50, 150,

757 200 µg/mL) in complete medium for 24–48 h. After treatment, cells were washed with warm
758 1× HBSS, and MTT (0.5 mg/mL) was added to each well. Plates were incubated in the dark
759 at 37 °C for 4 h. Formazan crystals were solubilized with 100 µL DMSO/well and gently
760 rocked for 15 min. Absorbance was recorded at 570 nm using a Varioskan multimode plate
761 reader (Thermo Scientific, USA). Cell viability was expressed as the OD (optical density) in
762 treated versus untreated cells.
763
764 ***Pressure Overload Cellular Model***
765 A pressure overload model was established using a weight-based method [26, 27].
766 Cardiomyoblasts were cultured in low-glucose DMEM with 10% FBS and antibiotics in 6-
767 well plates. After 24 h, differentiation was induced by incubating cells in 1% FBS medium
768 for 24 h. At ~80% confluence, medium was replaced with CO_2-independent medium
769 containing 5% FBS to minimize pH fluctuations under reduced gas exchange.
770 Mechanical stress was simulated by placing sterile 10 g weights (~1 g/cm²) on the medium
771 surface, applying consistent pressure to mimic pathological cardiomyocyte overload. Cells
772 were exposed to pressure for 12–48 h; controls (NO-PO) were cultured without weights but
773 covered with dummy lids to ensure equal gas exchange. PO enhanced the cell surface area of
774 cardiomyocytes by 3-4 fold, akin to that observed in the in vivo animal experiments.
775 Following treatment, three independent experiments per group (NO-PO and PO) received AR
776 (100 µg/mL) or GA (100 µM), doses determined via viability assays; three remained
777 untreated. Cells were harvested for analysis of hypertrophic markers, protein expression,
778 signaling pathways, and validation of mechanical load–induced hypertrophy.
779
780 ***Dot Blot ELISA***
781 Proteins were extracted using lysis buffer and quantified by BCA assay to normalize
782 concentrations. Equal amounts (6 µg in 2.2 µL) were spotted onto 0.45 µm nitrocellulose
783 membranes (Amersham), air-dried for 2 h at room temperature, and blocked overnight at 4 °C
784 with 3% BSA in TBST (0.1% Tween-20).Membranes were washed thrice with TBST,
785 incubated with primary antibodies diluted in blocking buffer for 1 h, followed by HRP-
786 conjugated secondary antibodies for 1 h at room temperature. Signals were detected using
787 enhanced chemiluminescence and imaged digitally. Dot intensities were quantified with Fiji
788 software to assess protein expression.
789
790

791 ***Human Galectin-3 ELISA***

792 Serum samples were diluted 1:1 and processed per the manufacturer's protocol. Absorbance
793 was measured at 450 nm using a Varioskan multimode plate reader (Thermo Scientific,
794 USA). Data represent mean ± SD from three independent experiments.

795

796 ***Immunocytochemistry***

797 Cells were fixed in 1.5% paraformaldehyde for 20 min, permeabilized with 0.25% saponin
798 for 20 min, and blocked for 1 h in PBS containing 3% BSA and 2% normal serum. Primary
799 antibodies were applied overnight at 4 °C. After PBS washes, cells were incubated with
800 Alexa Fluor–conjugated secondary antibodies (1:200; Jackson ImmunoResearch) for 1 h at
801 room temperature in the dark. Slides were mounted with DAPI-containing medium
802 (Invitrogen), and images were captured using an Olympus confocal microscope (60× oil
803 objective, NA 1.29). Imaging and analysis followed established protocols. Duolink in situ
804 proximity ligation assay was performed according to the manufacturer's instructions (Sigma,
805 USA)[54].

806

807 ***Western Blotting***

808 Cells were washed with 1× PBS and lysed in RIPA buffer (0.1% NP-40, 0.1% SDS, 0.5%
809 sodium deoxycholate, 150 mM NaCl, 50 mM Tris-HCl pH 7.4, protease inhibitors). Lysates
810 were sonicated and centrifuged at 14,000 rpm for 15 min at 4 °C; supernatants were collected.
811 Equal amounts of protein were mixed with SDS-β-mercaptoethanol sample buffer, heated at
812 95 °C for 5 min, separated by SDS-PAGE, and transferred to PVDF membranes.
813 Membranes were blocked overnight in TBST (0.1% Tween-20) with 3% BSA, then incubated
814 with primary antibodies diluted in blocking buffer for 1 h at room temperature or overnight at
815 4 °C. After washes, membranes were probed with HRP-conjugated secondary antibodies and
816 developed using Clarity ECL (Bio-Rad). Signals were detected with LAS-500 imaging
817 system.

818

819 ***Plasmid Transfection***

820 Cells at 70% confluence were incubated in serum-free OPTIMEM for 2 h prior to
821 transfection. High-purity plasmids (0.5 µg) were complexed with Lipofectamine LTX Plus
822 reagent at room temperature for 15–30 min. The mixture was then diluted with 350 µL
823 OPTIMEM and added dropwise to cells with gentle swirling. After 4–6 h incubation at 37 °C,

824 5% CO_2, the transfection medium was replaced with complete growth medium. Cells were
825 cultured for 24–72 h for optimal expression.
826
827 ***Galectin-3 WT and Mutant Conditioned Medium Experiments***
828 Cardiomyocytes were transfected with Gal-3 EGFP wild-type or carbohydrate recognition
829 domain mutant Gal-3 R186S EGFP plasmids. Following pressure overload treatment,
830 conditioned media containing secreted Gal-3 were collected. Cardiomyocytes were then
831 incubated with either Gal-3 EGFP or R186S EGFP media for 24 h. Cells were fixed in 1.5%
832 PFA for surface imaging or stained with rhodamine phalloidin to visualize F-actin stress
833 fibers.
834
835 ***Rhodamine Phalloidin and WGA Staining***
836 Fixed cells, prepared for immunocytochemistry if needed, were incubated with Rhodamine
837 phalloidin (2 µg/mL) for 45 min to visualize F-actin stress fibers. For WGA staining, cells
838 were treated with WGA (5 µg/mL) for 45 min, followed by brief washes. Cells were
839 counterstained with Hoechst (5 µg/mL, 5 min) and mounted. Imaging parameters and analysis
840 were consistent with prior protocols [54].
841
842 ***Cell Surface-Bound Galectin-3 Extraction via Acid Wash***
843 At the endpoint of PO and AR/GA treatments, media were collected, and plates with live
844 cells were placed on ice. Cells were incubated with complete medium adjusted to pH 2.0 for
845 45 minutes to strip surface-bound galectin-3. Released Gal-3 was analyzed from the acid
846 wash media normalized to normal pH, while cells were lysed separately to assess intracellular
847 Gal-3 levels.
848
849 ***Human Serum Conditioned Media Experiment***
850 Human serum was diluted in cardiomyocyte culture medium at 1:20, 1:40, and 1:60 ratios.
851 Differentiated cardiomyocytes were incubated with these dilutions for 10 hours before
852 fixation. Samples were then processed to assess cell surface area and detect surface-bound N-
853 and C-epitope galectin-3 by antibody staining.
854
855 ***Immunoprecipitation and Epitope Enrichment from Human Serum***
856 Selective enrichment of N- or C-epitope galectin-3 from aged human serum samples (n=3)
857 was performed using Dynabeads Protein A immunoprecipitation according to the

858 manufacturer's protocol. Dynabeads (1.5 mg) were conjugated with 4 µg of anti-N- or anti-C-
859 epitope galectin-3 antibodies. A total of 1600 µg serum protein (20 µl serum diluted in 580 µl
860 PBST) was incubated overnight at 4°C with antibody-conjugated beads on a rotator. The
861 following day, supernatants were collected, and 225 µl aliquots were incubated overnight at
862 4°C with or without 40 mM lactose.
863 Lactose-treated and untreated supernatants (225 µl each) were mixed 1:1 with cardiomyocyte
864 culture medium, and cardiomyocytes were incubated for 10 hours. Cells were then fixed, and
865 surface area was analyzed by capturing five random images per condition, quantifying
866 approximately 200 cells.
867 Equal volumes of supernatants were also analyzed by Western blot to confirm N- and C-
868 epitope enrichment, with the expectation of reciprocal enrichment (e.g., N-epitope bead pull-
869 down enriched for C-epitope in the supernatant).
870
871 ***Surface Visualization of N- and C-Epitope of Galectin-3***
872 To visualize surface-bound N- and C-epitope pools of galectin-3, fixed cells were incubated
873 with the respective antibodies for 45 minutes without permeabilization. For simultaneous
874 visualization of both epitopes on the same tissue section, primary antibodies (N-epitope-FITC
875 conjugated, C-epitope Alexa 594 conjugated) were applied sequentially, and signals were
876 developed.
877
878 ***Galectin-3 Docking and Simulation Studies with AR Components***
879 The carbohydrate-binding site of human Galectin-3 (Gal-3, PDB ID: 3ZSK) and a homology-
880 modeled structure of rat Gal-3 were prepared using the Schrödinger Protein Preparation
881 Wizard (Schrödinger Release 2021-3: Glide, Schrödinger, LLC, New York, NY, 2021). The
882 aim was to determine the binding conformations and energies of 18 compounds identified in
883 the Amalaki Rasayana (AR) extract. Receptor structures were energy-minimized with the
884 OPLS_2005 force field, constraining heavy atoms to deviate no more than 0.3 Å from their
885 original positions.
886 For molecular docking, Glide [55, 56, 57] was used to generate receptor grids centered on the
887 ligand-binding site defined by the human Gal-3 crystal structure, ensuring accurate
888 representation of the binding pocket. These grids served as docking targets for the selected
889 compounds.
890 The LigPrep module generated 3D structures of the 18 compounds, optimized their geometry,
891 and produced all possible stereoisomers and ionization states. The energy-minimized ligands

were docked into the receptor grids using Glide in standard precision (SP) mode with pre-defined constraints.

The docking protocol predicted the preferred conformation and orientation of each ligand within the receptor's binding site. The pose with the lowest GlideScore (GScore) was selected as the best-docked conformation and used for subsequent interaction analysis.

Statistics

All experiments were performed in triplicate, with error bars representing the standard deviation (SD) calculated from three independent experiments. Statistical significance for pairwise comparisons was determined using Bonferroni's t-test, with significance levels indicated as $*p \leq 0.05$, $**p \leq 0.01$, and $***p \leq 0.001$. Data are presented as means ± SD from a minimum of three independent trials.

For single-cell analyses, between 50 and 200 cells were quantified from five randomly selected fields per condition, across three independent experiments. Image analysis was conducted using Fiji software, and calibration bars for LUT-converted images are included in the corresponding figures.

DECLARATIONS:

Ethics approval and consent to participate.

Not applicable.

Consent for publication

Not applicable.

Availability of data and materials

All data generated during the current study are available in the manuscript itself, including un-cropped, original western and dot representative images.

Funding

The work is supported by Indian Council of Medical Research (ICMR) extramural research grant (File no. 2020-0169/CMB/ADHOC-BMS).

CRediT authorship contribution statement

Puja Laxmanrao Shinde: Methodology, Formal analysis, Investigation, Visualization. **Vikas Kumar:** Methodology, Formal analysis. **Siddhartha Singh:** Methodology, Formal analysis, Investigation, Visualization. **K.C. Sivakumar :** Methodology, Formal analysis, Investigation. **Rashmi Mishra:** Conceptualization, Methodology, Formal analysis, Resources, Investigation, Visualization, Supervision, Project administration, Funding acquisition, Writing – review & editing.

Declaration of competing interest

The authors declare that they have no known competing financial interests.

Acknowledgments

PLS and SS acknowledge research fellowships from the Department of Biotechnology (DBT) and University Grant Commission (UGC), respectively.

REFERENCES

1. Hein, S. et al. Progression from compensated hypertrophy to failure in the pressure-overloaded human heart. *Circulation* 107, 984–991 (2003).
2. Norton, G. R. et al. Heart failure in pressure overload hypertrophy. The relative roles of ventricular remodeling and myocardial dysfunction. *J. Am. Coll. Cardiol.* 39, 664–671 (2002).
3. Beslika, E. et al. Large animal models of pressure overload-induced cardiac left ventricular hypertrophy to study remodelling of the human heart with aortic stenosis. *Cardiovasc. Res.* 120, 461–475 (2024).
4. Vigil-Garcia, M. et al. Gene expression profiling of hypertrophic cardiomyocytes identifies new players in pathological remodelling. *Cardiovasc. Res.* 117, 1532–1545 (2021).
5. Meijers, W. C. et al. Circulating heart failure biomarkers beyond natriuretic peptides: review from the Biomarker Study Group of the Heart Failure Association (HFA), European Society of Cardiology (ESC). *Eur. J. Heart Fail.* 23, 1610–1632 (2021).
6. Berezin, A. E. & Berezin, A. A. Biomarkers in heart failure: from research to clinical practice. *Ann. Lab. Med.* 43, 225–236 (2023).
7. McCullough, P. A., Olobatoke, A. & Vanhecke, T. E. Galectin-3: a novel blood test for the evaluation and management of patients with heart failure. *Rev. Cardiovasc. Med.* 12, 200–210 (2011).
8. Lopez-Andrès, N. et al. Association of galectin-3 and fibrosis markers with long-term cardiovascular outcomes in patients with heart failure. *Eur. J. Heart Fail.* 14, 74–81 (2012).
9. Sharma, U. C. et al. Galectin-3 marks activated macrophages in failure-prone hypertrophied hearts and contributes to cardiac dysfunction. *Circulation* 110, 3121–3128 (2004).

10. de Boer, R. A. et al. Galectin-3: a novel mediator of heart failure development and progression. *Eur. J. Heart Fail.* 11, 811–817 (2009).
11. McCullough, P. A. Practical experience using galectin-3 in heart failure. *Clin. Chem. Lab. Med.* 52, 1425–1431 (2014).
12. Zaborska, B. et al. The role of galectin-3 in heart failure—the diagnostic, prognostic and therapeutic potential. *Int. J. Mol. Sci.* 24, 13111 (2023).
13. Dumic, J., Dabelic, S. & Flögel, M. Galectin-3: an open-ended story. *Biochim. Biophys. Acta* 1760, 616–635 (2006).
14. Lepur, A. et al. Ligand induced galectin-3 protein self-association. *J. Biol. Chem.* 287, 21751–21756 (2012).
15. Halimi, H. et al. Glycan dependence of galectin-3 self-association properties. *PLoS One* 9, e111836 (2014).
16. Suthahar, N. et al. Galectin-3 activation and inhibition in heart failure and cardiovascular disease: an update. *Theranostics* 8, 593–609 (2018).
17. Variya, B. C., Bakrania, A. K. & Patel, S. S. *Emblica officinalis* (Amla): a review for its phytochemistry, ethnomedicinal uses and medicinal potentials. *Pharmacol. Res.* 111, 180–200 (2016).
18. Kumar, V. et al. Amalakirasayana, a traditional Indian drug enhances cardiac mitochondrial and contractile functions in rats with hypertrophy. *Sci. Rep.* 7, 8588 (2017).
19. Kumar, V. et al. Untargeted metabolomics reveals alterations in lipid metabolism and immune pathways after long-term administration of Amalaki rasayana. *Mol. Cell. Biochem.* 463, 147–160 (2020).
20. Rai, A. et al. Mapping drug-target interactions and synergy in multi-molecular therapeutics for pressure-overload cardiac hypertrophy. *NPJ Syst. Biol. Appl.* 7, 11 (2021).
21. Yan, X. et al. Gallic acid suppresses cardiac hypertrophic remodeling and heart failure. *Mol. Nutr. Food Res.* 63, e1800807 (2019).
22. Jin, L. et al. Gallic acid improves cardiac dysfunction and fibrosis in pressure overload-induced heart failure. *Sci. Rep.* 8, 9302 (2018).
23. Jayakody, R. S. et al. Bergenin: a computationally proven promising scaffold for novel galectin-3 inhibitors. *J. Mol. Model.* 24, 302 (2018).
24. Chauhan, R. et al. Bergenin inhibits growth of human cervical cancer cells by decreasing galectin-3 and MMP-9 expression. *Sci. Rep.* 14, 15287 (2024).
25. Salomonsson, E. et al. Mutational tuning of galectin-3 specificity and biological function. *J. Biol. Chem.* 285, 35079–35091 (2010).
26. Kanzaki, H. et al. Periodontal ligament cells under mechanical stress induce osteoclastogenesis by RANKL up-regulation via PGE2 synthesis. *J. Bone Miner. Res.* 17, 210–220 (2002).
27. Nazet, U. et al. Housekeeping gene validation for RT-qPCR studies on synovial fibroblasts. *PLoS One* 14, e0225790 (2019).
28. Bänfer, S. et al. Molecular mechanism to recruit galectin-3 into multivesicular bodies for polarized exosomal secretion. *Proc. Natl Acad. Sci. USA* 115, E4396–E4405 (2018).
29. Mehul, B. & Hughes, R. C. Plasma membrane targeting, vesicular budding and release of galectin-3. *J. Cell Sci.* 110, 1169–1178 (1997).
30. Mazurek, N. et al. Phosphorylation of galectin-3 modulates binding to its ligands. *J. Biol. Chem.* 275, 36311–36315 (2000).
31. Liu, F. et al. Mechanism of regulation of casein kinase I activity by group I metabotropic glutamate receptors. *J. Biol. Chem.* 277, 45393–45399 (2002).

32. Ippel, H. et al. Intra- and intermolecular interactions of human galectin-3: assessment by full-assignment-based NMR. *Glycobiology* 26, 888–903 (2016).
33. Zhang, Q. et al. Signaling pathways and targeted therapy for myocardial infarction. *Signal Transduct. Target. Ther.* 7, 78 (2022).
34. Kilian, L. S. et al. RhoA: a dubious molecule in cardiac pathophysiology. *J. Biomed. Sci.* 28, 33 (2021).
35. Sotodosos-Alonso, L. et al. Caveolae mechanotransduction at the interface between cytoskeleton and extracellular matrix. *Cells* 12, 942 (2023).
36. Liu, S. et al. Design and synthesis of dual galectin-3 and EGFR inhibitors against liver fibrosis. *Chem. Asian J.* 20, e202401078 (2025).
37. Yang, E. H. et al. Galectin-3 alters the lateral mobility and clustering of β1-integrin receptors. *PLoS One* 12, e0184378 (2017).
38. Troncoso, M. F. et al. The universe of galectin-binding partners and their functions in health and disease. *J. Biol. Chem.* 299, 105400 (2023).
39. Joeh, E. et al. Mapping glycan-mediated galectin-3 interactions by live cell proximity labeling. *Proc. Natl Acad. Sci. USA* 117, 27329–27338 (2020).
40. Joshi, B. et al. Phosphocaveolin-1 is a mechanotransducer that induces caveola biogenesis via Egr1 transcriptional regulation. *J. Cell Biol.* 199, 425–435 (2012).
41. Zimnicka, A. M. et al. Src-dependent phosphorylation of caveolin-1 Tyr-14 promotes swelling and release of caveolae. *Mol. Biol. Cell* 27, 2090–2106 (2016).
42. Hatch, E. M. & Hetzer, M. W. Nuclear envelope rupture is induced by actin-based nucleus confinement. *J. Cell Biol.* 215, 27–36 (2016).
43. Elosegui-Artola, A. et al. Force triggers YAP nuclear entry by regulating transport across nuclear pores. *Cell* 171, 1397–1410.e14 (2017).
44. Osmanagic-Myers, S., Dechat, T. & Foisner, R. Lamins at the crossroads of mechanosignaling. *Genes Dev.* 29, 225–237 (2015).
45. Kessler-Icekson, G. et al. ANP expression in the hypertensive heart. *Exp. Clin. Cardiol.* 7, 80–84 (2002).
46. Cao, M. et al. Role of CyPA in cardiac hypertrophy and remodeling. *Biosci. Rep.* 39, BSR20193190 (2019).
47. Cao, M. et al. Extracellular cyclophilin A induces cardiac hypertrophy via the ERK/p47phox pathway. *Mol. Cell. Endocrinol.* 518, 110990 (2020).
48. Prenner, S. B. et al. Serum albumin is a marker of myocardial fibrosis, adverse pulsatile aortic hemodynamics, and prognosis in HFpEF. *J. Am. Heart Assoc.* 9, e014716 (2020).
49. Wu, N. et al. Albuminuria is associated with left ventricular hypertrophy in patients with early diabetic kidney disease. *Int. J. Endocrinol.* 2014, 351945 (2014).
50. de Boer, R. A. et al. Predictive value of plasma galectin-3 levels in heart failure with reduced and preserved ejection fraction. *Ann. Med.* 43, 60–68 (2011).
51. Ibrahim, N. E. & Januzzi, J. L. Established and emerging roles of biomarkers in heart failure. *Circ. Res.* 123, 614–629 (2018).
52. Sciacchitano, S. et al. Galectin-3: one molecule for an alphabet of diseases, from A to Z. *Int. J. Mol. Sci.* 19, 379 (2018).
53. Portacci, A. et al. Galectin-3 as prognostic biomarker in patients with COVID-19 acute respiratory failure. *Respir. Med.* 187, 106556 (2021).
54. *Neurotherapeutic implications of sense and respond strategies generated by astrocytes and astrocytic tumours to combat pH mechanical stress. Neuropathol. Appl. Neurobiol.* 48, e12774 (2022).
55. Friesner, R. A. et al. Extra precision glide: docking and scoring incorporating a model of hydrophobic enclosure. *J. Med. Chem.* 49, 6177–6196 (2006).

56. Halgren, T. A. et al. Glide: a new approach for rapid, accurate docking and scoring. 2. Enrichment factors in database screening. *J. Med. Chem.* 47, 1750–1759 (2004).
57. Friesner, R. A. et al. Glide: a new approach for rapid, accurate docking and scoring. 1. Method and assessment of docking accuracy. *J. Med. Chem.* 47, 1739–1749 (2004).

FIGURE LEGENDS:

Figure 1. Development and validation of an Amalaki Rasayana (AR)-based therapeutic model for left ventricular cardiac hypertrophy (CH).

(A) Experimental design: Age-matched rat groups included BA (21-month-old biologically aged rats with mild age-related CH), BA+AR (BA rats treated with AR from 9 to 21 months, totaling 12 months), PO-CH (rats subjected to trans-aortic constriction at 3 months, developing pressure overload-induced CH by 9 months and ventricular dilation by 21 months), and PO-CH+AR (PO-CH rats treated with AR for ≥12 months post-surgery, from 9 to 21 months).

(B–D) M-mode echocardiography assessing left ventricular ejection fraction (LVEF), fractional shortening (LVFS), and ventricular dimensions showed significant improvement in AR-treated groups compared to untreated BA and PO-CH cohorts.

(E) Exercise tolerance tests measuring fatigue time indicated enhanced cardiac output in AR-treated rats versus untreated groups.

(F, G, J, K) Immunohistochemistry for CD68+ macrophages and αSMA+ activated fibroblasts revealed significant reductions in AR-treated animals relative to controls.

(H, L) Sirius red staining demonstrated decreased myocardial fibrosis in AR-treated groups.

(I, M) Alizarin S staining indicated reduced myocardial calcification with AR treatment.

Data represent mean ± SD; significance: *$p < 0.05$, **$p < 0.01$, ***$p < 0.001$; n = 4–8 rats per group.

Figure 2. Additional validation of the Amalaki Rasayana (AR)-based therapeutic model for left ventricular cardiac hypertrophy (CH).

(A) Representative cross-sectional images of the left ventricular wall in 21-month-old PO-CH rats displaying dilated hypertrophic cardiomyopathy.

(B) AR-treated BA and PO-CH rats exhibited reduced cellular loss and thicker ventricular walls compared to untreated counterparts, at the end of 21st month.

1100 **(C–F)** Wheat germ agglutinin (WGA) staining and analysis of cardiomyocyte surface area
1101 revealed decreased hypertrophy in AR-treated BA and PO-CH rats across endocardial,
1102 myocardial, and pericardial layers.
1103 **(G)** Although cardiomyocytes from untreated BA and PO-CH groups had larger surface
1104 areas, they showed reduced biomass, indicated by lower total protein (Amido Black staining)
1105 and RNA content (Pyronin Y staining) per cell, relative to AR-treated cohorts (measured over
1106 5 random ROIs).
1107 **(K)** Serum levels of LDHA and HMGB1, markers of plasma membrane permeability and cell
1108 injury, were decreased in AR-treated groups, consistent with reduced cell loss observed in
1109 panels (A, B).
1110 Dot blot protein analysis demonstrated gene expression shifts in AR-treated rats: decreased
1111 fetal cardiac markers (ANP, GATA4, MYH7, MEF2A), increased adult cardiac muscle
1112 proteins (cTNT, ACTN2, TMOD1, OBSCN, SERCA2A), and reduced hypertrophy-
1113 associated proteins (CAMK2D, CaNA, NFATC2) compared to untreated BA and PO-CH
1114 groups.
1115 X-axis numerals in graphs correspond to: 1=BA, 2=BA+AR, 3=PO-CH, 4=PO-CH+AR.
1116 Data are mean ± SD; significance: *$p < 0.05$, **$p < 0.01$, ***$p < 0.001$; n = 8 rats/group.
1117 Image acquisition parameters were consistent across all conditions; single-cell analyses
1118 included 30–60 cells per independent experiment.
1119
1120 **Figure 3. AR treatment reduces excessive galectin-3 C-epitope oligomer formation in**
1121 **cardiac hypertrophy.**
1122 **(A, B)** Dot blot assay using a knockout-validated anti-galectin-3 antibody targeting full-
1123 length protein (aa 1–250) shows comparative galectin-3 levels in serum from BA, BA+AR,
1124 PO-CH, and PO-CH+AR groups (n = 4); each spot contains 6 µg serum.
1125 **(C, D)** Western blot quantification of full-length galectin-3 reveals differential monomer and
1126 oligomer enrichment across groups.
1127 **(E)** Analysis of 60 µg serum from PO-CH rats with epitope-specific antibodies indicates
1128 enrichment of C-epitope-containing galectin-3 in dimeric and oligomeric forms in the
1129 hypertrophy model. The N-epitope antibody recognizes N-N homo-dimers, homo-oligomers,
1130 and monomeric/oligomeric full-length protein; the C-epitope antibody recognizes C-C homo-
1131 dimers, homo-oligomers, and monomeric/oligomeric full-length protein.
1132 **(F, G)** Western blot validation confirms differences in monomeric and oligomeric C-epitope
1133 galectin-3 pools between AR-treated and untreated BA and PO-CH rats.

1134 Data are mean ± SD; significance by t-test: *p ≤ 0.05, **p ≤ 0.01, ***p ≤ 0.001.

1135

1136 **Figure 4. Predominance of galectin-3 C-epitope oligomers in cardiac hypertrophy.**

1137 **(A)** Schematic of the in vitro cellular pressure overload (PO) model, created with
1138 Biorender.com

1139 **(B, C)** Representative rhodamine phalloidin-stained images and quantification of
1140 cardiomyocyte surface area following incubation with galectin-3 WT-EGFP or carbohydrate-
1141 binding mutant (Gal3 R186S, CRD-MUT) under no pressure overload (No-PO) and PO
1142 conditions.

1143 **(D–F)** Analysis of surface-bound galectin-3 WT-EGFP and CRD-MUT-EGFP on
1144 cardiomyocytes, including binding patterns, signal intensity, and cluster area under No-PO
1145 and PO conditions.

1146 Data are mean ± SD; significance by t-test: *p ≤ 0.05, **p ≤ 0.01, ***p ≤ 0.001.

1147

1148 **Figure 5. AR treatment significantly reduces extracellular galectin-3 C-epitope**
1149 **oligomers in vitro and in vivo.**

1150 **(A)** MTT assay assessing cardiomyocyte viability with increasing AR doses over 24 hours;
1151 no viability increase observed above 100 µg/ml.

1152 **(B)** Cardiomyocytes subjected to 24-hour pressure overload (PO) were treated with 100
1153 µg/ml AR for an additional 24 hours; AR treatment significantly increased cell counts
1154 compared to No-PO and PO alone.

1155 **(C–H)** Western blot analysis quantifying monomeric and oligomeric galectin-3 C-epitope
1156 levels in culture media (C, D), surface-bound fractions (E, F), and intracellular lysates (G, H)
1157 under conditions described in (B). Surface galectin-3 was isolated via low pH wash.

1158 **(I)** Representative 4× images of surface-bound galectin-3 C-epitope clusters in left
1159 ventricular tissues from BA and PO-CH rats, showing high clustering in PO-CH.

1160 **(J–L)** Comparative quantification of galectin-3 N- and C-epitope surface levels in BA and
1161 PO-CH tissues with or without AR treatment; untreated PO-CH tissues exhibit significant C-
1162 epitope clustering.

1163 Graph and blot labeling: 1=BA, 2=BA+AR, 3=PO-CH, 4=PO-CH+AR.

1164 Data are mean ± SD; n ≥ 4 animals/group; significance by t-test: *p ≤ 0.05, **p ≤ 0.01, ***p
1165 ≤ 0.001.

1166

1167 **Figure 6. Validation of elevated extracellular galectin-3 C-epitope oligomers in**
1168 **hypertrophic cardiomyopathy (HCM) donor cardiomyocytes versus normal controls.**
1169 **(A, B)** Human cardiac tissues from normal and HCM donors were stained for surface-bound
1170 galectin-3 N-epitope (cyan) and C-epitope (magenta). Merged images reveal significantly
1171 reduced N and C-epitope co-localization in HCM cardiomyocytes compared to normal tissue,
1172 indicating predominance of C-C homo-oligomers over N-N or full-length galectin-3.
1173 Wheat germ agglutinin (WGA, green) marks cardiomyocyte surfaces. Merged images of C-
1174 epitope and WGA highlight prominent galectin-3 C-epitope clusters (white arrowheads) on
1175 HCM cardiomyocytes.
1176 Data are mean ± SD; significance by t-test: *$p \leq 0.05$, **$p \leq 0.01$, ***$p \leq 0.001$.
1177
1178 **Figure 7. Gallic acid (GA) from AR extract reduces excess extracellular galectin-3 C-**
1179 **epitope oligomers.**
1180 **(A)** Glide docking scores of 18 key AR components with rat and human galectin-3.
1181 **(B)** Molecular dynamics simulation showing GA forming hydrogen bonds with three critical
1182 residues (Arg144, Asn160, Asn164) in the galectin-3 carbohydrate recognition domain
1183 (CRD).
1184 **(C)** MTT assay assessing cardiomyocyte viability with increasing GA concentrations over 24
1185 hours; no significant viability increase above 100 μM GA.
1186 **(D)** Cardiomyocytes subjected to 24-hour pressure overload (PO) were treated with 100 μM
1187 GA for 24 hours; GA treatment significantly increased cell counts compared to No-PO and
1188 PO alone.
1189 **(E–J)** Western blot analysis quantifying monomeric and oligomeric galectin-3 C-epitope
1190 levels in culture media (E, F), surface-bound fractions (G, H), and intracellular lysates (I, J)
1191 under conditions described in (D). Surface galectin-3 was isolated via low pH wash.
1192 X-axis labeling: 1=BA, 2=BA+GA, 3=PO-CH, 4=PO-CH+GA.
1193 Data are mean ± SD; significance by t-test: *$p \leq 0.05$, **$p \leq 0.01$, ***$p \leq 0.001$.
1194
1195 **Figure 8. Gallic acid (GA) in AR reduces galectin-3 release by promoting N-epitope**
1196 **phosphorylation and cytoplasmic retention.**
1197 **(A–C)** GA, AR, and BAPTA-AM treatments reduce extracellular galectin-3 C-epitope
1198 oligomer cluster area and intensity on cardiomyocyte surfaces under pressure overload (PO)
1199 and no-PO conditions.

1200 **(D, E)** Proximity ligation assay (PLA) shows increased galectin-3 phosphorylation and
1201 intracellular retention in AR- and GA-treated cardiomyocytes. BAPTA-AM–mediated
1202 calcium reduction enhances phosphorylation and retention, suggesting calcium regulates
1203 galectin-3 secretion and intracellular loss.
1204 **(F, G)** PLA quantification of phosphorylated galectin-3 in BA and PO-CH rat tissues with or
1205 without AR treatment; untreated PO-CH tissues show significantly lower phosphorylation.
1206 **(H, I)** PLA analysis comparing normal human left ventricular and hypertrophic
1207 cardiomyopathy (HCM) tissues reveals reduced phosphorylated galectin-3 in HCM
1208 cardiomyocytes.
1209 **(J, K)** Immunoprecipitation (IP) with anti-galectin-3 and western blotting mediated immuno-
1210 detection with pan phosphoserine antibodies demonstrates enhanced intracellular galectin-3
1211 phosphorylation in GA-treated cardiomyocytes.
1212 **(L, M)** IP of GFP-tagged WT galectin-3 from PO ± GA cardiomyocytes shows increased
1213 phosphorylation with GA; no change is observed with S6 mutant (that inhibits serine
1214 phosphorylation at 6th position in N-epitope), triple mutant that inhibits GA-binding in the
1215 CRD, indicating GA binds galectin-3 CRD and modulates phosphorylation at N-epitope S6.
1216 No change in phosphorylation is observed in IP samples expressing either only C- or N-
1217 epitope, again suggesting that GA influences N-epitope serine phosphorylation by binding to
1218 the C-epitope.
1219 **(N–P)** Incubation of fresh cardiomyocytes with lactose-pretreated media from WT-GFP
1220 galectin-3–expressing PO cardiomyocytes reduces surface galectin-3 binding in a dose-
1221 dependent manner, indicating GA inhibits glycan binding of extracellular galectin-3, akin to
1222 lactose.
1223 Data are mean ± SD; $n \geq 4$ animals or 3 independent experiments; significance by t-test: $*p \leq$
1224 0.05, $**p \leq 0.01$, $***p \leq 0.001$.
1225
1226 **Figure 9. Validation of galectin-3 C-epitope oligomers in human donor serum samples.**
1227 **(A–D)** Serum from young individuals, older adults, and cardiac hypertrophy survivors (post
1228 various pharmacological treatments) was analyzed for ANP and galectin-3 epitope levels.
1229 **(E)** Galectin-3 concentrations in these sera were quantified by a commercial ELISA kit,
1230 wherein the plates were coated using a full-length anti-galectin-3 antibody.
1231 Statistical significance was assessed by t-tests: $*p \leq 0.05$, $**p \leq 0.01$, $***p \leq 0.001$.
1232
1233

1234 **Figure 10. Validation of dominant galectin-3 C-epitope oligomers in cardiomyocyte**
1235 **hypertrophy over N-epitope.**
1236 **(A, B)** Rat cardiomyocytes treated with sera from young, old, and cardiac hypertrophy
1237 survivors at varying dilutions were stained with rhodamine-phalloidin to assess cell surface
1238 area and visualize stress fibers, which increase under mechanical stress.
1239 **(C, D)** Galectin-3 C- and N-epitope pools were immunoprecipitated from human old donor
1240 sera. Pre-incubation with lactose or vehicle was performed before conditioning
1241 cardiomyocytes with these pools. Changes in cell surface area and stress fiber formation were
1242 quantified, showing C-epitope-enriched sera induced hypertrophy, which lactose attenuated.
1243 **(E, F)** Immunofluorescence analysis revealed differential cell surface binding patterns of Gal-
1244 3 C- and N-epitope pools, with C-epitope exhibiting clustered organization and inducing
1245 prominent stress fibers, modulated by lactose treatment.
1246 Keys to histogram bar colours and numericals used on the X-axis of the graphs are provided
1247 within the figure. Statistical significance was evaluated by t-tests: *$p \leq 0.05$, **$p \leq 0.01$, ***p
1248 ≤ 0.001.
1249
1250 **Figure 11. Human galectin-3 C-epitope oligomers play a dominant role in cardiac**
1251 **hypertrophy and cardiomyocyte loss.**
1252 Human galectin-3 C- and N-epitope pools were immunoprecipitated from old donor sera and
1253 applied to cardiomyocytes at a 1:40 dilution. Parallel treatments involved pre-mixing these
1254 epitopes with 40 mM lactose or gallic acid (GA) before cell incubation.
1255 **(A, B)** C-epitope formed distinct surface clusters, which were absent when pre-incubated
1256 with lactose or GA, while N-epitope exhibited a diffuse surface distribution.
1257 **(C, D)** C-epitope induced increased F-actin stress fibers and cell surface area (hypertrophy),
1258 effects blocked by lactose or GA.
1259 **(E–G)** Upregulation of RhoA-ROCK1 signaling was observed with C-epitope treatment but
1260 attenuated by lactose or GA.
1261 **(H, I)** Loss of membrane tension buffering structures, caveolae, was visualized via reduced
1262 PLA signal intensity between CAV-1 and PTRF, as PTRF dissociated from CAV1 during
1263 caveolae disassembly.
1264 **(J, K)** Increased nuclear localization of YAP1, a mechanotransduction transcription factor,
1265 was induced by C-epitope and mitigated by lactose or GA.
1266 **(L, M)** Nuclear membrane stiffening was evidenced by increased Lamin-A levels.
1267 **(N, O)** Elevated DNA damage was shown by intense γ phospho-H2AX staining.

1268 **(P–S)** Expression of hypertrophy-associated genes NFATC2 and MEF2 was increased.
1269 **(T, U)** Cardiomyocyte permeability increased, as measured by extracellular levels of LDHA
1270 (an endogenous enzyme), in culture media.
1271 Numerical keys on the X-axis: 1 =Gal-3 C- or N-epitope enriched pool, whichever applicable
1272 (generated through IP from old human donor), 2 = Gal-3 C- or N-epitope enriched pool
1273 premixed with lactose (+ Lactose/+L), 3 = Gal-3 C- or N-epitope enriched pool premixed
1274 with gallic acid (+ Gallic acid/+GA).
1275 Statistical significance was assessed by t-tests: *$p \leq 0.05$, **$p \leq 0.01$, ***$p \leq 0.001$.
1276
1277 **Figure 12. Graphical summary illustrating that excessively secreted galectin-3 C-epitope**
1278 **oligomers represent a critical drug target in cardiac hypertrophy (CH).**
1279 **1.** During CH, cardiomyocyte plasma membranes undergo dynamic hydrostatic
1280 pressure-induced stretching. This mechanical stretch activates calcium-conducting
1281 pressure/stretch sensors, increasing intracellular calcium influx. Elevated calcium activates
1282 calcineurin A (CaNA), a phosphatase that dephosphorylates casein kinase 1 (CKI). CKI
1283 normally phosphorylates galectin-3 at serine residues (notably serine 6 in the N-domain), a
1284 modification that promotes intracellular retention of galectin-3 and limits its secretion.
1285 However, CaNA-mediated CKI inactivation reduces galectin-3 phosphorylation, leading to
1286 increased secretion of unphosphorylated galectin-3 into the extracellular space.
1287 **2.** Extracellular galectin-3 is proteolytically cleaved into N- and C-domains by enzymes
1288 such as matrix metalloproteinases. These domains homo-oligomerize and multimerize on the
1289 cardiomyocyte surface, with C-epitope oligomers forming large clusters that induce intense
1290 biomechanical stress. This mechanical stress activates the RhoA-ROCK pathway, promoting
1291 the formation of rigid F-actin stress fibers that help withstand membrane tension but
1292 compress and deform the nucleus, causing chromatin damage.
1293 **3.** These stress fibers also cause the disassembly of caveolae—the cell's primary
1294 membrane tension-buffering structures—by removing their PTRF coat, increasing membrane
1295 tension, loss of permeability, and ultimately cell death.
1296 **4.** The RhoA-ROCK pathway further activates PTEN phosphatase, converting PIP3 to
1297 PIP2. PIP2 stimulates PLC, triggering DAG-MAPK signaling and nuclear translocation of
1298 hypertrophy-associated transcription factors (MEF2, GATA4). PLC also promotes IP3-
1299 mediated calcium release from intracellular stores, amplifying intracellular calcium and
1300 calcineurin A activation, which drives further secretion of unphosphorylated galectin-3.

1301 **5.** Elevated calcium also activates CAMK2A autophosphorylation, causing additional
1302 calcium release from intracellular stores and CAMK2A nuclear translocation, which
1303 promotes hypertrophy gene expression.
1304 **6.** High calcium levels, through calcineurin A, dephosphorylate NFATC2, facilitating its
1305 nuclear translocation and upregulation of hypertrophy genes, resulting in cardiomyocyte
1306 overstretch and death.
1307 **Therapeutic mechanism:**
1308 AR extract and its bioactive component gallic acid (GA) bind to the carbohydrate recognition
1309 domain (CRD) of galectin-3, inducing a conformational change that enhances CKI
1310 accessibility to the galectin-3 N-domain. This increases galectin-3 phosphorylation,
1311 promoting intracellular retention and reducing harmful extracellular secretion. Additionally,
1312 AR and GA bind extracellular galectin-3 CRD, blocking its surface clustering and the
1313 subsequent activation of the RhoA-ROCK1-PTEN-PLC-Ca^{2+} signaling cascade, thereby
1314 mitigating calcium dysregulation and cellular damage.
1315
1316 **Figure 13: Correlated reduction of galectin-3 C-epitope levels with ANP, PPIA, and**
1317 **ALB in AR-treated rats.**
1318 Dot blot assays measuring **(B, F)** galectin-3 C-epitope and its putative interaction partners—
1319 **(A, E)** atrial natriuretic peptide (ANP), **(C, G)** peptidylprolyl isomerase A (PPIA), and **(D, H)**
1320 albumin (ALB)—in serum samples from BA, BA+AR, PO-CH, and PO-CH+AR rat cohorts
1321 (n=4 per group). Each dot corresponds to 6 µg of serum protein and was probed using
1322 knockout-validated antibodies specific to each target. Data are presented as mean ± SD, with
1323 statistical significance assessed by t-tests; $*p \leq 0.05$, $**p \leq 0.01$, $***p \leq 0.001$
1324
1325
1326 **Figure 14: Quantification of PPIA and ALB levels in human sera.**
1327 **(A, B, C, D)** Serum samples from young individuals, older adults, and cardiac hypertrophy
1328 survivors receiving diverse pharmacological treatments were analyzed for peptidylprolyl
1329 isomerase A (PPIA) and albumin (ALB) levels. Data are shown as mean ± SD, with
1330 statistical significance determined by t-tests; $*p \leq 0.05$, $**p \leq 0.01$, $***p \leq 0.001$
1331
1332 **Figure 15: Summary of the research findings.**
1333 Aging and pressure overload-driven cardiac hypertrophy result in elevated tissue and
1334 circulating levels of galectin-3 C-epitope oligomers, ANP, PPIA, and ALB—key proteins

1335 implicated in cardiac damage. Treatment with Amalaki Rasayana (AR) or gallic acid (GA)
1336 leads to significant improvements in cardiac function, morphology, cellular and molecular
1337 parameters, alongside marked reductions in galectin-3 C-epitope oligomers, PPIA, ANP, and
1338 ALB levels. These proteins collectively serve as a biomarker panel to monitor therapeutic
1339 efficacy. Additionally, AR/GA-mediated inhibition of excessive extracellular galectin-3 C-
1340 epitope oligomers attenuates cellular tension, RhoA-ROCK1 signaling, formation of rigid F-
1341 actin stress fibers, loss of caveolae, hypertrophy gene expression, cardiomyocyte surface
1342 area, DNA damage, and cell death.
1343
1344 **FIGURES 1-15 (From Page 39-53)**

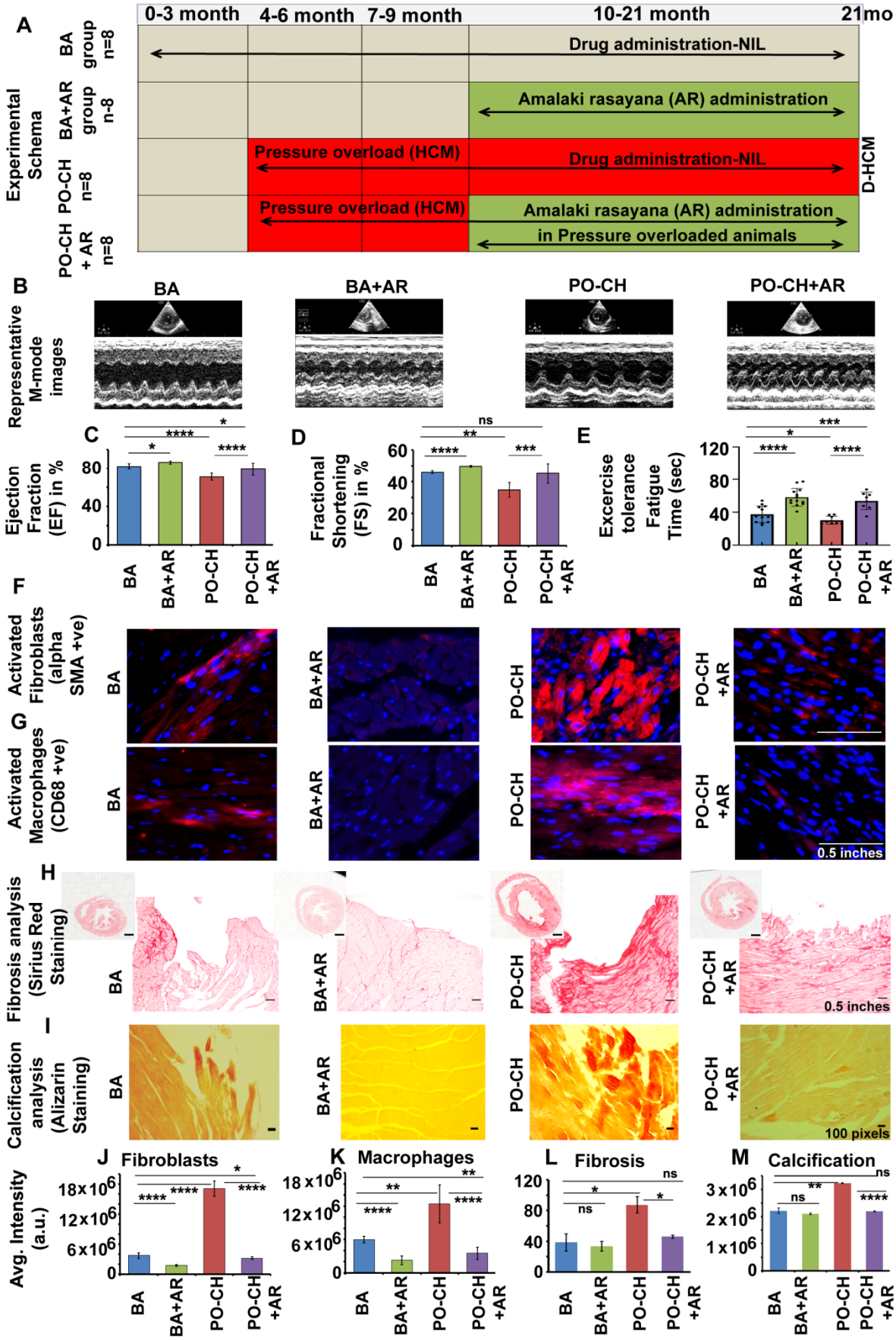
A
0-3 month
4-6 month
7-9 month
10-21 month
21mo
Experimental Schema
BA group n=8
Drug administration-NIL
BA+AR group n-8
Amalaki rasayana (AR) administration
PO-CH n=8
Pressure overload (HCM)
Drug administration-NIL
D-HCM
PO-CH + AR n=8
Pressure overload (HCM)
Amalaki rasayana (AR) administration in Pressure overloaded animals
B
BA
BA+AR
PO-CH
PO-CH+AR
Representative M-mode images
C
Ejection Fraction (EF) in %
D
Fractional Shortening (FS) in %
E
Excercise tolerance Fatigue Time (sec)
F
Activated Fibroblasts (alpha SMA +ve)
G
Activated Macrophages (CD68 +ve)
0.5 inches
H
Fibrosis analysis (Sirius Red Staining)
0.5 inches
I
Calcification analysis (Alizarin Staining)
100 pixels
Avg. Intensity (a.u.)
J Fibroblasts
K Macrophages
L Fibrosis
M Calcification

FIGURE 1

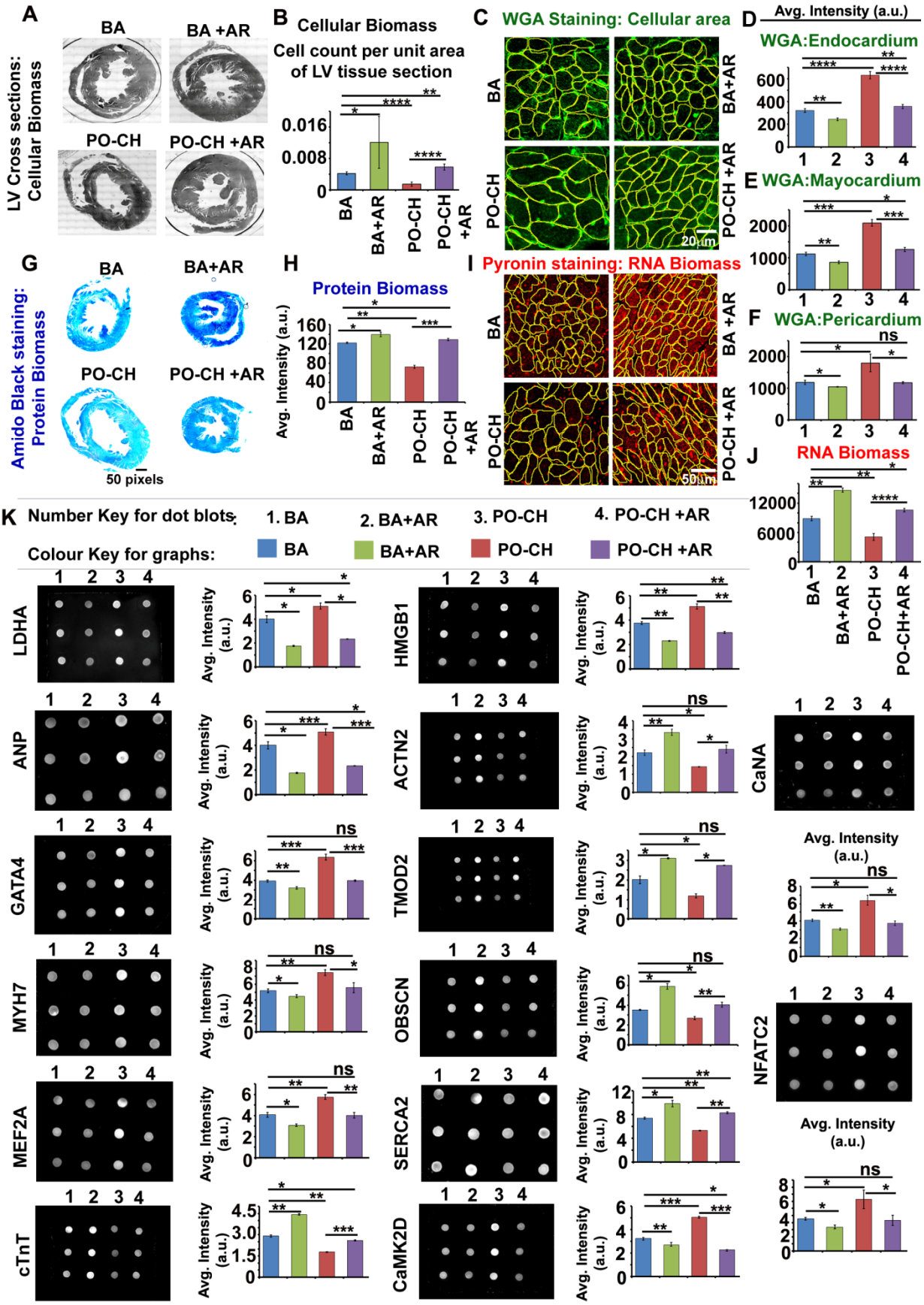
A
LV Cross sections: Cellular Biomass
BA
BA +AR
PO-CH
PO-CH +AR
B Cellular Biomass
Cell count per unit area of LV tissue section
0.016
0.008
0
BA
BA+AR
PO-CH
PO-CH +AR
C WGA Staining: Cellular area
20 µm
D Avg. Intensity (a.u.)
WGA:Endocardium
E WGA:Mayocardium
F WGA:Pericardium
G
Amido Black staining: Protein Biomass
50 pixels
H
Protein Biomass
Avg. Intensity (a.u.)
I Pyronin staining: RNA Biomass
50 µm
J
RNA Biomass
K Number Key for dot blots:
1. BA
2. BA+AR
3. PO-CH
4. PO-CH +AR
Colour Key for graphs:
LDHA
HMGB1
ANP
ACTN2
CaNA
GATA4
TMOD2
MYH7
OBSCN
NFATC2
MEF2A
SERCA2
cTnT
CaMK2D
Avg. Intensity (a.u.)
ns

FIGURE 2

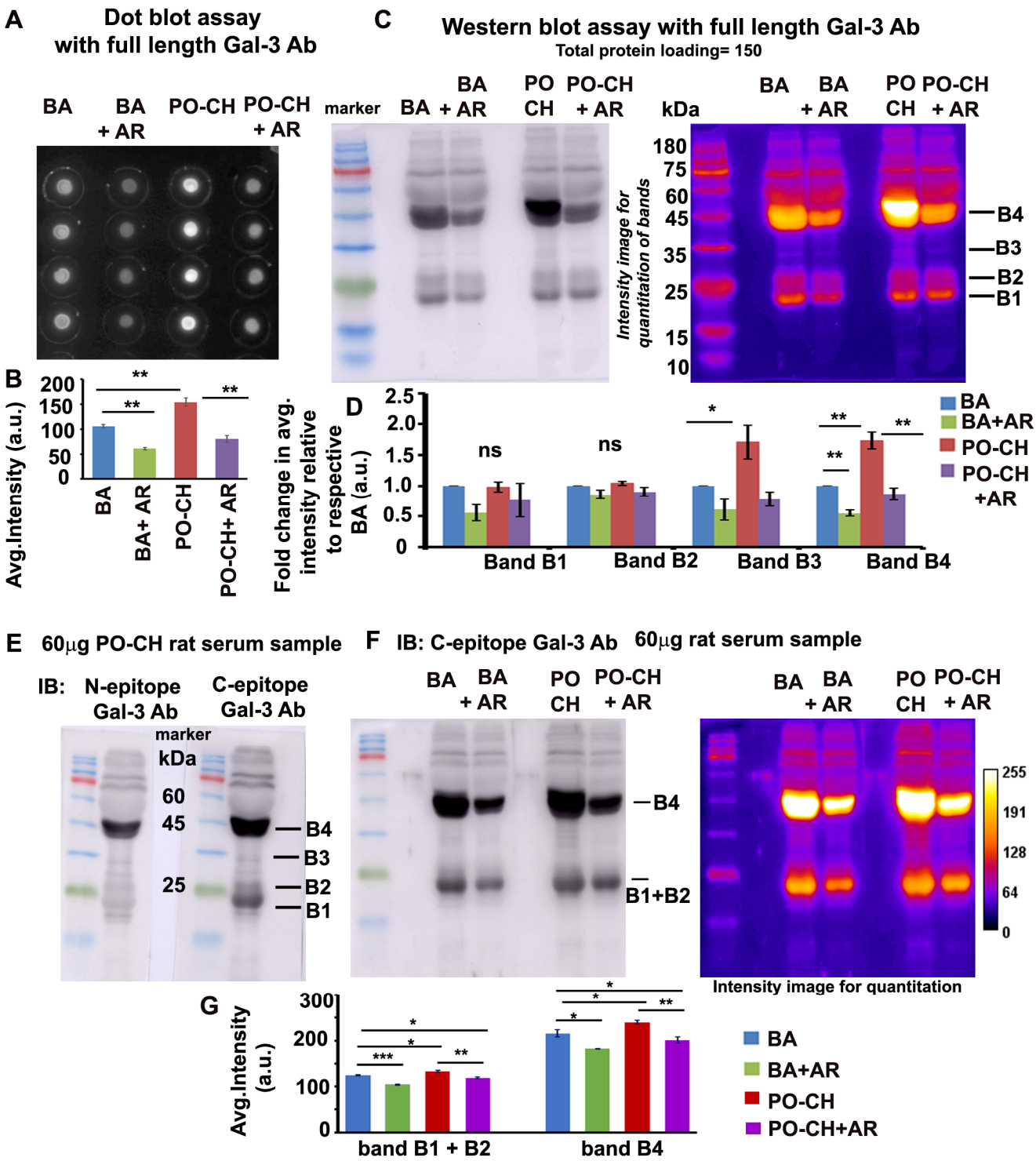
A
Dot blot assay
with full length Gal-3 Ab
BA
BA + AR
PO-CH
PO-CH + AR
C
Western blot assay with full length Gal-3 Ab
Total protein loading= 150
marker
BA
BA + AR
PO CH
PO-CH + AR
kDa
180
75
60
45
35
25
15
10
Intensity image for quantitation of bands
B4
B3
B2
B1
B
Avg.Intensity (a.u.)
200
150
100
50
0
BA
BA+ AR
PO-CH
PO-CH+ AR
D
Fold change in avg. intensity relative to respective BA (a.u.)
2.5
2.0
1.5
1.0
0.5
0
ns
Band B1
Band B2
Band B3
Band B4
BA
BA+AR
PO-CH
PO-CH +AR
E
60μg PO-CH rat serum sample
IB:
N-epitope Gal-3 Ab
C-epitope Gal-3 Ab
marker
kDa
60
45
25
B4
B3
B2
B1
F
IB: C-epitope Gal-3 Ab
60μg rat serum sample
BA
BA + AR
PO CH
PO-CH + AR
B4
B1+B2
255
191
128
64
0
Intensity image for quantitation
G
Avg.Intensity (a.u.)
300
200
100
0
band B1 + B2
band B4
BA
BA+AR
PO-CH
PO-CH+AR

FIGURE 3

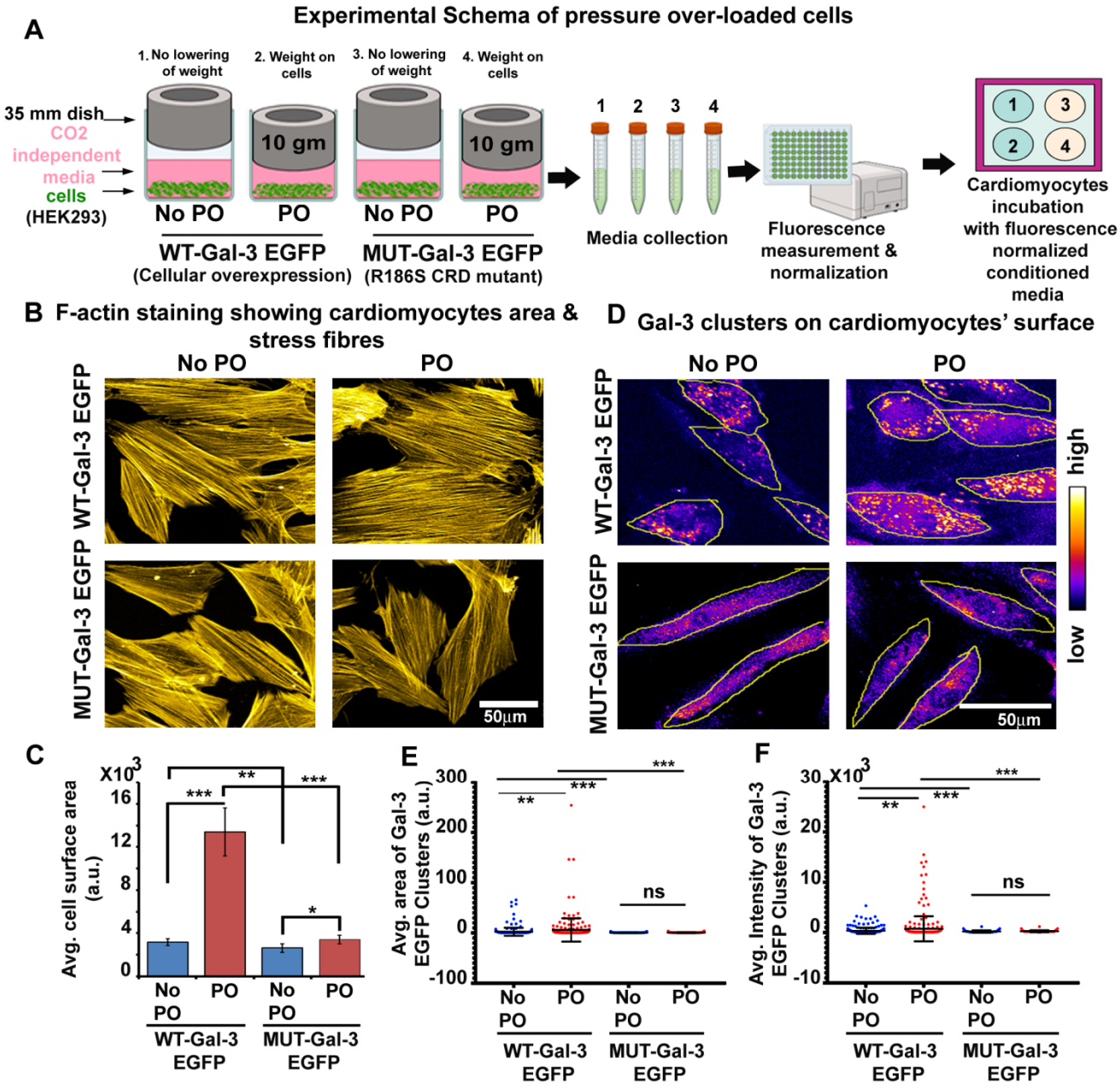
A
Experimental Schema of pressure over-loaded cells
1. No lowering of weight
2. Weight on cells
3. No lowering of weight
4. Weight on cells
35 mm dish
CO2 independent media
cells
(HEK293)
10 gm
10 gm
No PO
PO
No PO
PO
WT-Gal-3 EGFP
(Cellular overexpression)
MUT-Gal-3 EGFP
(R186S CRD mutant)
1 2 3 4
Media collection
Fluorescence measurement & normalization
Cardiomyocytes incubation with fluorescence normalized conditioned media
B F-actin staining showing cardiomyocytes area & stress fibres
No PO
PO
WT-Gal-3 EGFP
MUT-Gal-3 EGFP
50µm
D Gal-3 clusters on cardiomyocytes' surface
No PO
PO
WT-Gal-3 EGFP
MUT-Gal-3 EGFP
high
low
50µm
C
Avg. cell surface area (a.u.)
X10^3
16
12
8
4
0
***
**
***
*
No PO
PO
No PO
PO
WT-Gal-3 EGFP
MUT-Gal-3 EGFP
E
Avg. area of Gal-3 EGFP Clusters (a.u.)
300
200
100
0
-100
**
***
***
ns
No PO
PO
No PO
PO
WT-Gal-3 EGFP
MUT-Gal-3 EGFP
F
Avg. Intensity of Gal-3 EGFP Clusters (a.u.)
X10^3
30
20
10
0
-10
**
***
***
ns
No PO
PO
No PO
PO
WT-Gal-3 EGFP
MUT-Gal-3 EGFP

FIGURE 4

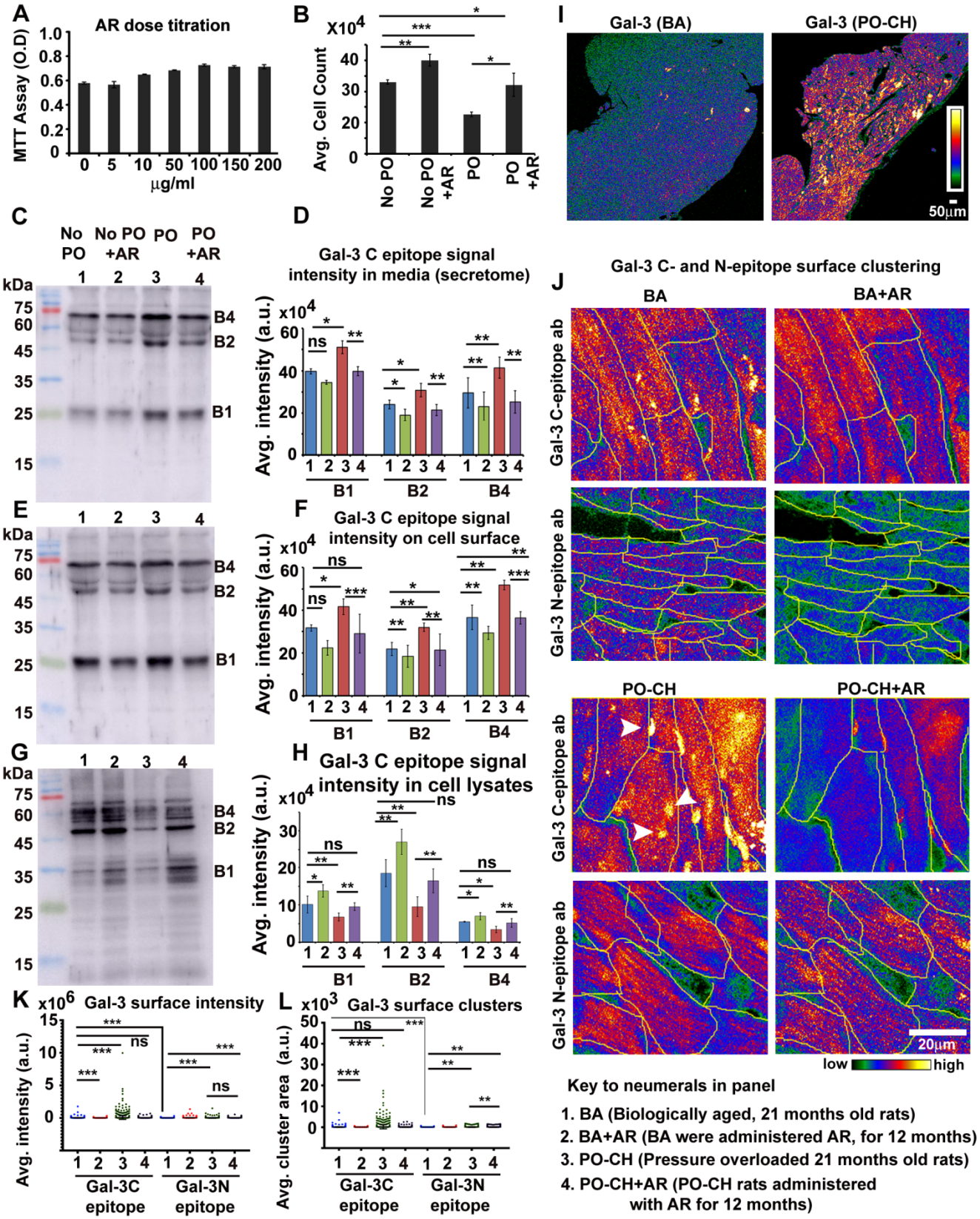
A
AR dose titration
MTT Assay (O.D)
1.0
0.8
0.6
0.4
0.2
0
0 5 10 50 100 150 200
µg/ml
B
X10^4
Avg. Cell Count
40
30
20
0
No PO
No PO +AR
PO
PO +AR
I
Gal-3 (BA)
Gal-3 (PO-CH)
50µm
C
No PO
No PO +AR
PO
PO +AR
1 2 3 4
kDa
75
60
45
35
25
15
B4
B2
B1
D
Gal-3 C epitope signal intensity in media (secretome)
x10^4
Avg. intensity (a.u.)
60
40
20
0
1 2 3 4 1 2 3 4 1 2 3 4
B1
B2
B4
E
1 2 3 4
kDa
75
60
45
35
25
15
B4
B2
B1
F
Gal-3 C epitope signal intensity on cell surface
x10^4
Avg. intensity (a.u.)
60
40
20
0
1 2 3 4 1 2 3 4 1 2 3 4
B1
B2
B4
G
1 2 3 4
kDa
75
60
45
35
25
15
B4
B2
B1
H
Gal-3 C epitope signal intensity in cell lysates
x10^4
Avg. intensity (a.u.)
30
20
10
0
1 2 3 4 1 2 3 4 1 2 3 4
B1
B2
B4
J
Gal-3 C- and N-epitope surface clustering
BA
BA+AR
PO-CH
PO-CH+AR
Gal-3 C-epitope ab
Gal-3 N-epitope ab
20µm
low
high
K
x10^6
Gal-3 surface intensity
Avg. intensity (a.u.)
15
10
5
0
1 2 3 4 1 2 3 4
Gal-3C epitope
Gal-3N epitope
L
x10^3
Gal-3 surface clusters
Avg. cluster area (a.u.)
50
40
30
20
10
0
1 2 3 4 1 2 3 4
Gal-3C epitope
Gal-3N epitope
Key to neumerals in panel
1. BA (Biologically aged, 21 months old rats)
2. BA+AR (BA were administered AR, for 12 months)
3. PO-CH (Pressure overloaded 21 months old rats)
4. PO-CH+AR (PO-CH rats administered with AR for 12 months)

FIGURE 5

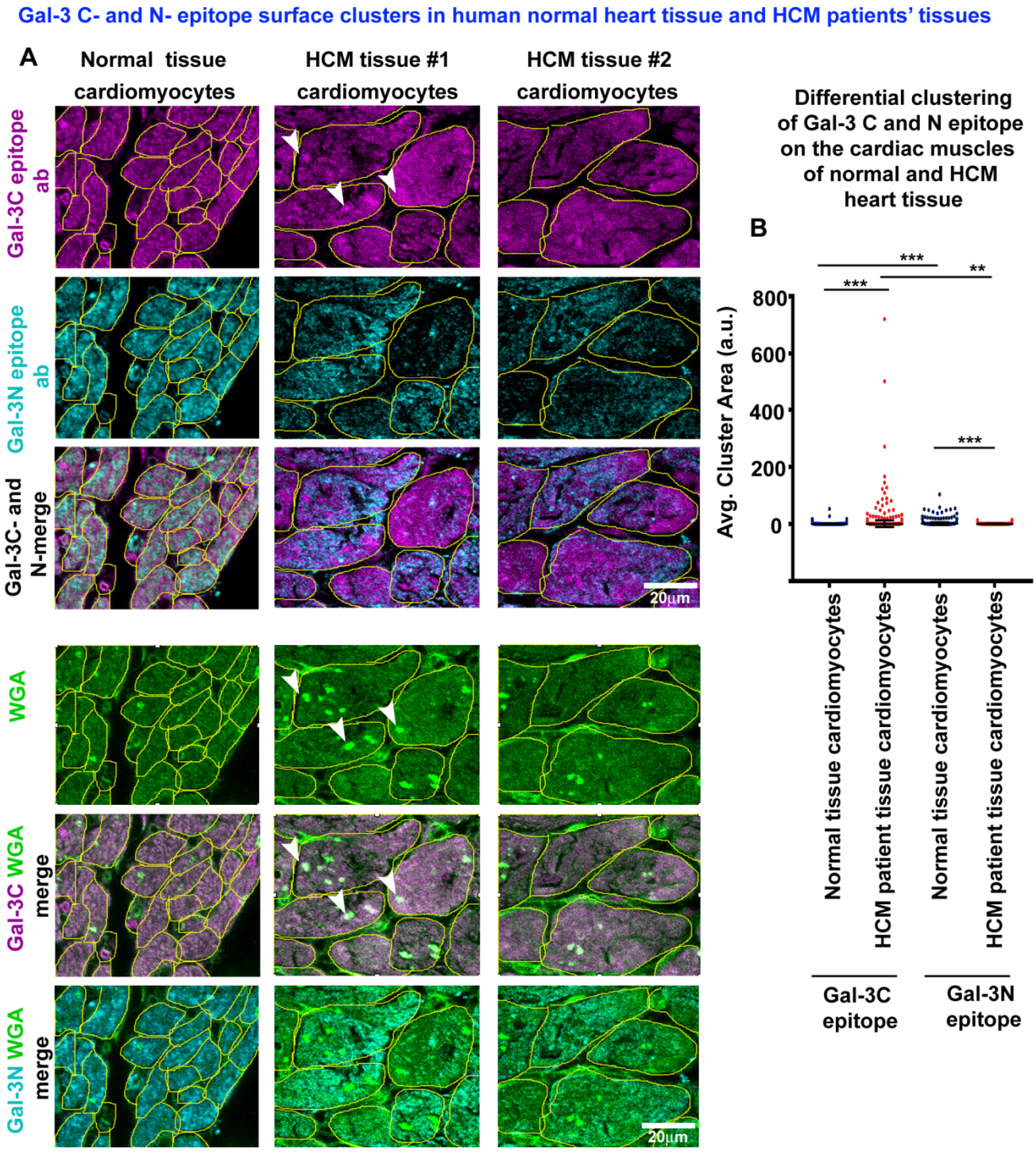
Gal-3 C- and N- epitope surface clusters in human normal heart tissue and HCM patients' tissues
A
Normal tissue cardiomyocytes
HCM tissue #1 cardiomyocytes
HCM tissue #2 cardiomyocytes
Gal-3C epitope ab
Gal-3N epitope ab
Gal-3C- and N-merge
WGA
Gal-3C WGA merge
Gal-3N WGA merge
20µm
20µm
Differential clustering of Gal-3 C and N epitope on the cardiac muscles of normal and HCM heart tissue
B
Avg. Cluster Area (a.u.)
800
600
400
200
0
***
***
**
***
Normal tissue cardiomyocytes
HCM patient tissue cardiomyocytes
Normal tissue cardiomyocytes
HCM patient tissue cardiomyocytes
Gal-3C epitope
Gal-3N epitope

FIGURE 6

A Glide score of docking between Galectin-3 and AR components

	Human Gal-3	Rat Gal-3
Pyridoxamine phosphate	-7.324	-4.632 *
Norepinephrine sulphate	-6.602	-5.615 *
Cabamoyl phosphate	-6.426	-4.669 *
Gallic acid	-6.191	-4.871 *
Nicotinate D-ribnucleoside	-6.16	-5.606 *
Cyclic 3',5'-guanylic acid	-5.878	-4.367
ProstaglandinB1	-5.754	-3.944
Ellagic acid	-5.028	-4.288
1,24,25-TrihydroxyvitaminD3	-4.95	-4.147
Cholic acid	-4.945	-4.844 *
5-Formiminotetrahydrofolate	-4.868	-4.158
5,6-Ep-15S-HETE	-4.802	-4.158

B Docking of Gallic acid in CRD of Gal-3

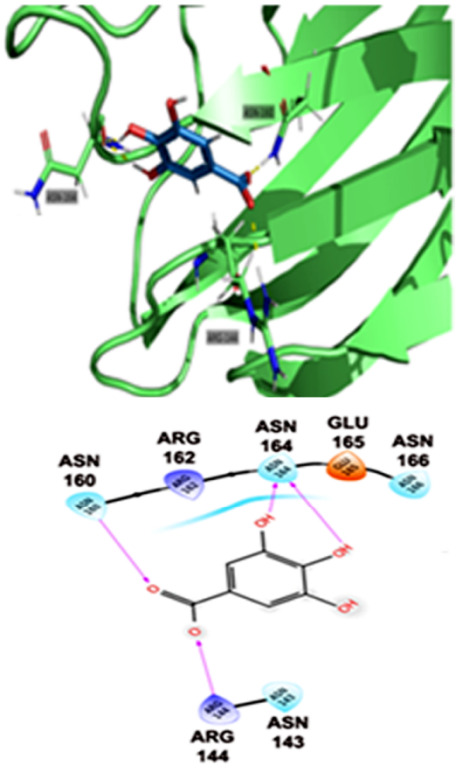

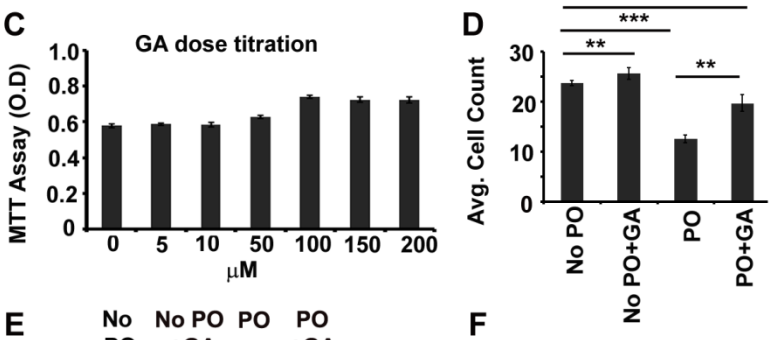

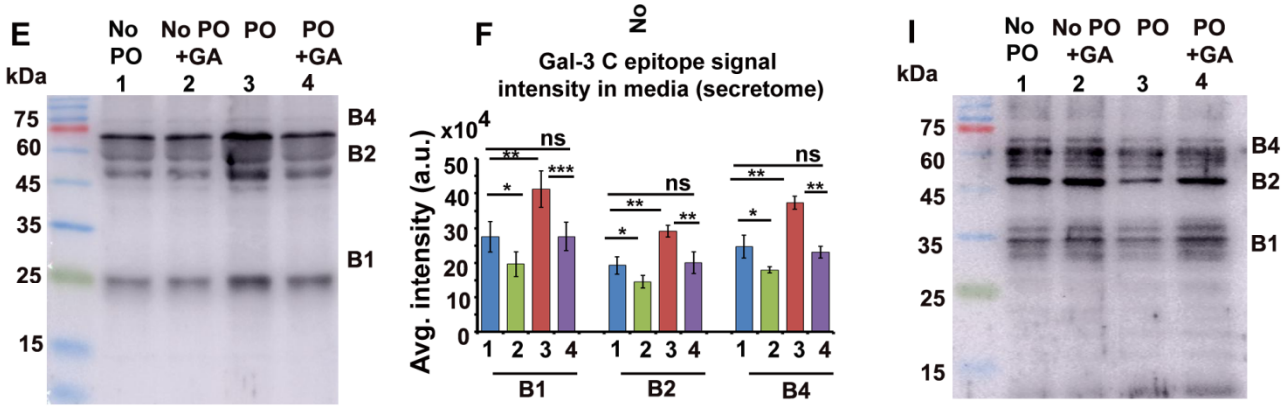

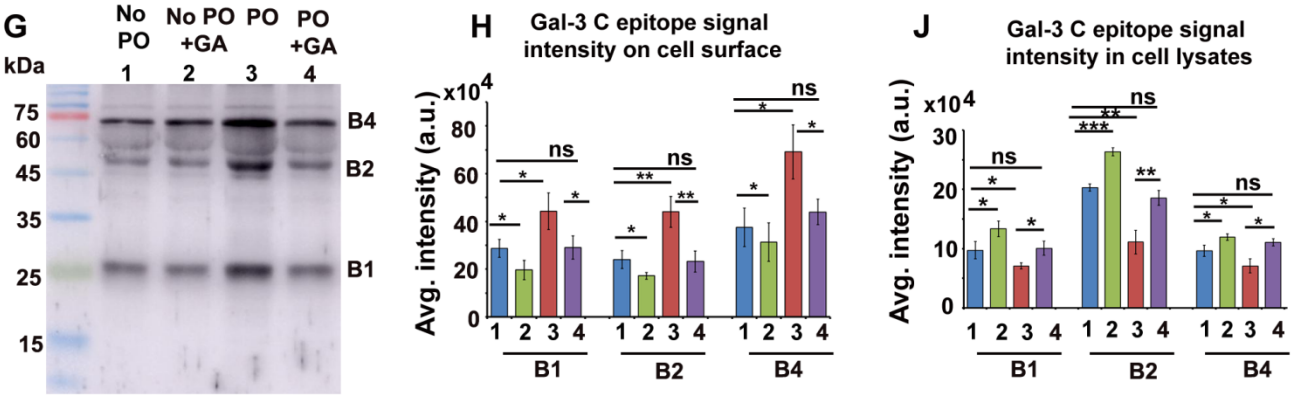

FIGURE 7

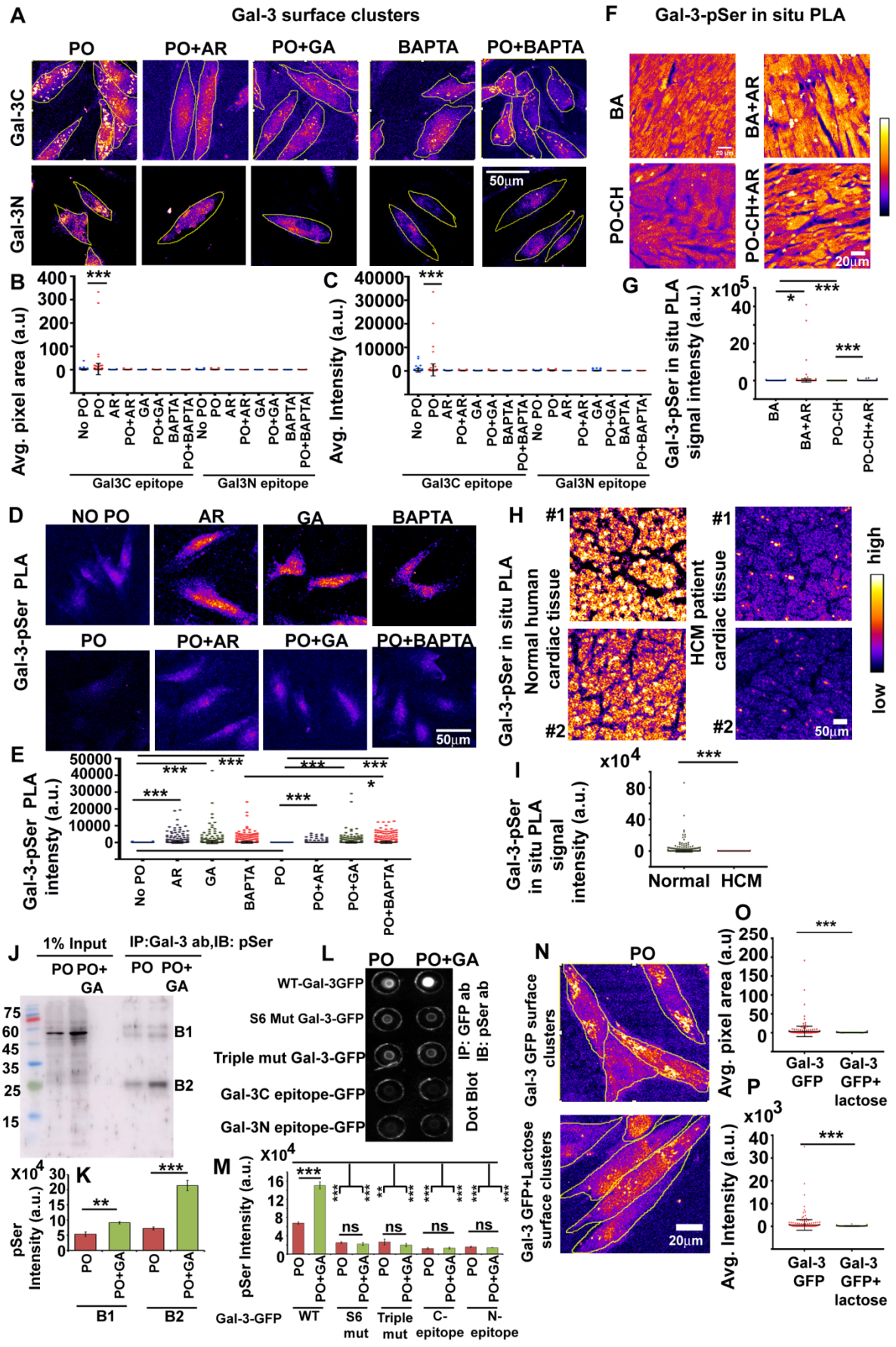
A
Gal-3 surface clusters
PO
PO+AR
PO+GA
BAPTA
PO+BAPTA
Gal-3C
Gal-3N
50µm
B
Avg. pixel area (a.u)
Gal3C epitope
Gal3N epitope
C
Avg. Intensity (a.u.)
F
Gal-3-pSer in situ PLA
BA
BA+AR
PO-CH
PO-CH+AR
20µm
G
Gal-3-pSer in situ PLA signal intensity (a.u.)
D
NO PO
AR
GA
BAPTA
Gal-3-pSer PLA
E
Gal-3-pSer PLA intensty (a.u.)
H
Gal-3-pSer in situ PLA
Normal human cardiac tissue
HCM patient cardiac tissue
#1
#2
high
low
I
Gal-3-pSer in situ PLA signal intensity (a.u.)
Normal
HCM
J
1% Input
IP:Gal-3 ab,IB: pSer
B1
B2
K
pSer Intensity (a.u.)
L
WT-Gal-3GFP
S6 Mut Gal-3-GFP
Triple mut Gal-3-GFP
Gal-3C epitope-GFP
Gal-3N epitope-GFP
IP: GFP ab
IB: pSer ab
Dot Blot
M
pSer Intensity (a.u.)
Gal-3-GFP
WT
S6 mut
Triple mut
C-epitope
N-epitope
N
Gal-3 GFP surface clusters
Gal-3 GFP+Lactose surface clusters
O
Avg. pixel area (a.u)
Gal-3 GFP
Gal-3 GFP+ lactose
P
Avg. Intensity (a.u.)

FIGURE 8

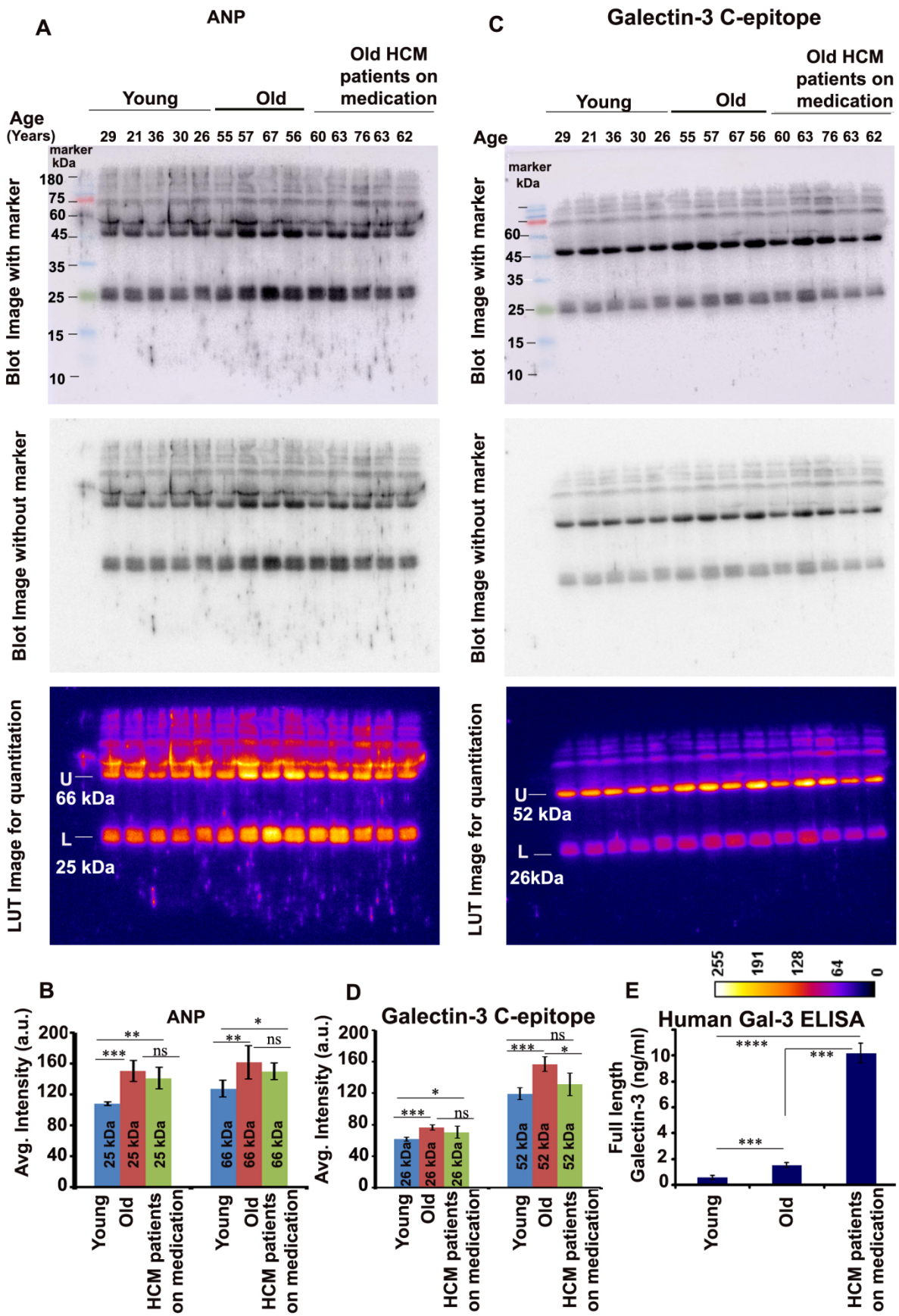
A
ANP
Young
Old
Old HCM patients on medication
Age (Years)
29 21 36 30 26 55 57 67 56 60 63 76 63 62
marker kDa
180
75
60
45
35
25
15
10
Blot Image with marker
Blot Image without marker
LUT Image for quantitation
U
66 kDa
L
25 kDa
C
Galectin-3 C-epitope
Young
Old
Old HCM patients on medication
Age
29 21 36 30 26 55 57 67 56 60 63 76 63 62
marker kDa
60
45
35
25
15
10
Blot Image with marker
Blot Image without marker
LUT Image for quantitation
U
52 kDa
L
26kDa
255
191
128
64
0
B
ANP
Avg. Intensity (a.u.)
200
160
120
80
40
0
**
***
ns
*
**
ns
25 kDa
25 kDa
25 kDa
66 kDa
66 kDa
66 kDa
Young
Old
HCM patients on medication
Young
Old
HCM patients on medication
D
Galectin-3 C-epitope
Avg. Intensity (a.u.)
200
160
120
80
40
0
*
***
ns
ns
***
*
26 kDa
26 kDa
26 kDa
52 kDa
52 kDa
52 kDa
Young
Old
HCM patients on medication
Young
Old
HCM patients on medication
E
Human Gal-3 ELISA
Full length Galectin-3 (ng/ml)
10
8
6
4
2
0
****
***
***
Young
Old
HCM patients on medication

FIGURE 9

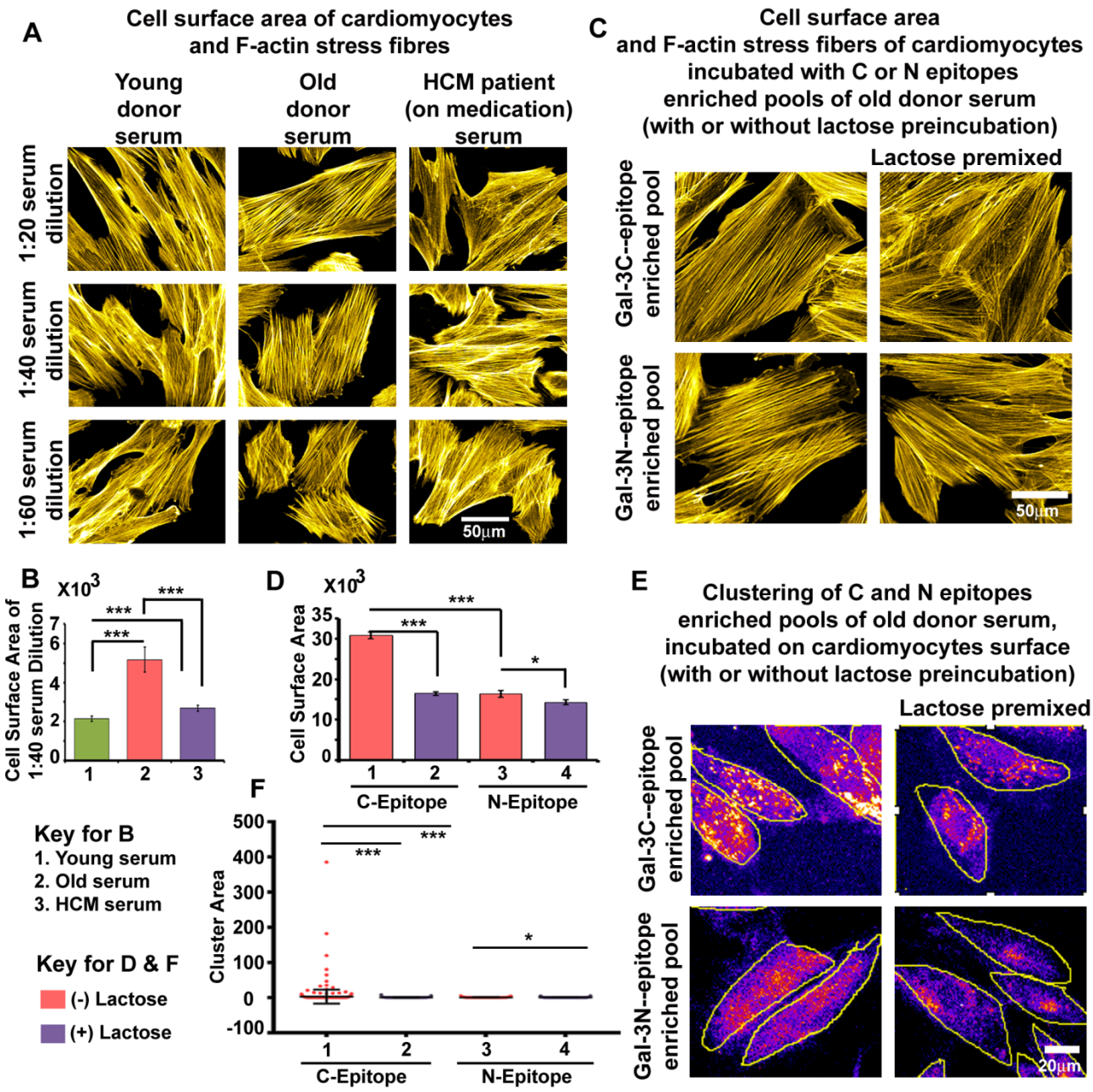
A
Cell surface area of cardiomyocytes and F-actin stress fibres
Young donor serum
Old donor serum
HCM patient (on medication) serum
1:20 serum dilution
1:40 serum dilution
1:60 serum dilution
50µm
C
Cell surface area and F-actin stress fibers of cardiomyocytes incubated with C or N epitopes enriched pools of old donor serum (with or without lactose preincubation)
Lactose premixed
Gal-3C--epitope enriched pool
Gal-3N--epitope enriched pool
50µm
B
X10^3
Cell Surface Area of 1:40 serum Dilution
***
***
***
1
2
3
D
X10^3
Cell Surface Area
***
***
*
1
2
3
4
C-Epitope
N-Epitope
E
Clustering of C and N epitopes enriched pools of old donor serum, incubated on cardiomyocytes surface (with or without lactose preincubation)
Lactose premixed
Gal-3C--epitope enriched pool
Gal-3N--epitope enriched pool
20µm
F
Cluster Area
***
***
*
1
2
3
4
C-Epitope
N-Epitope
Key for B
1. Young serum
2. Old serum
3. HCM serum
Key for D & F
(-) Lactose
(+) Lactose

FIGURE 10

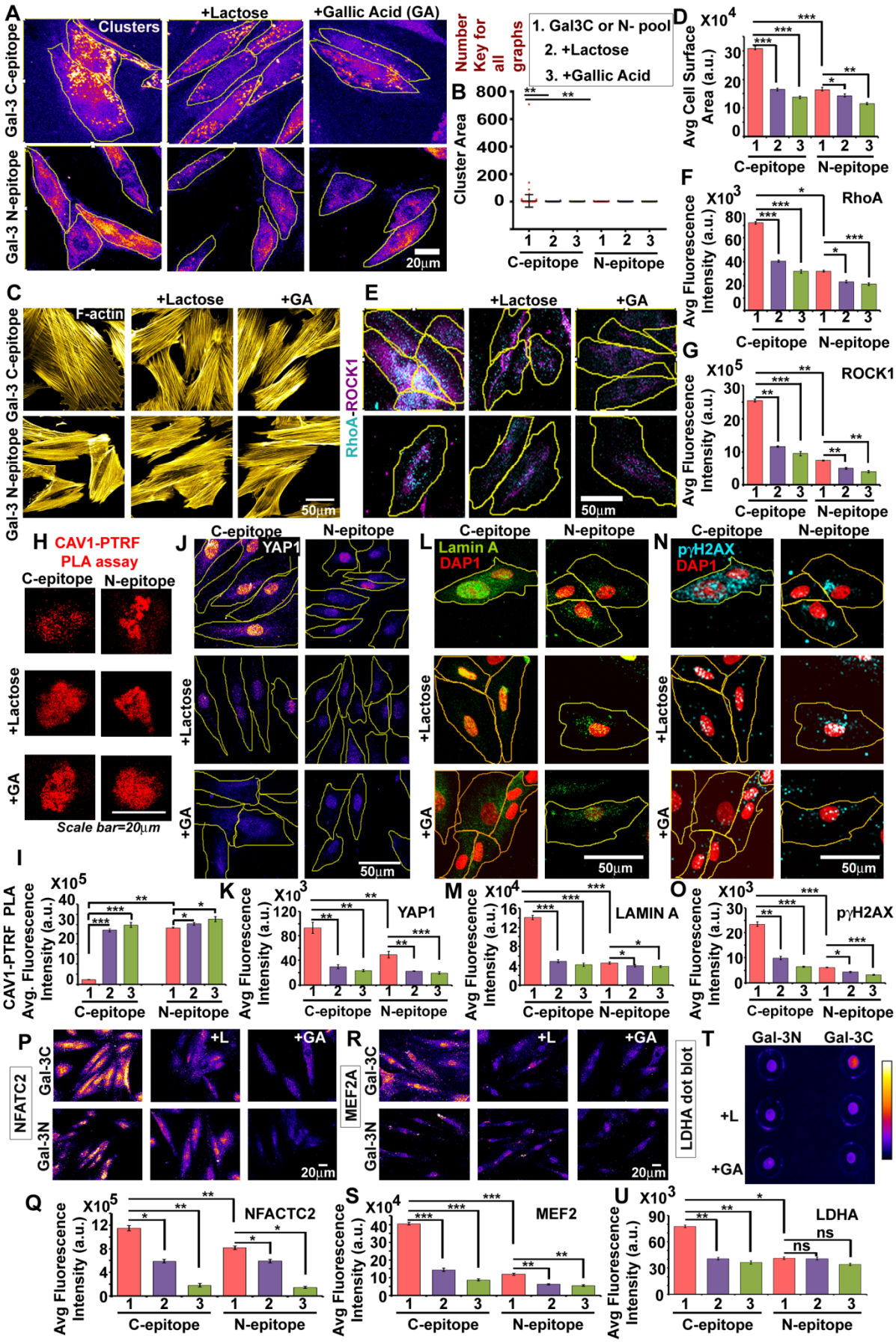
A
+Lactose
+Gallic Acid (GA)
Clusters
Gal-3 C-epitope
Gal-3 N-epitope
20µm
Number Key for all graphs
1. Gal3C or N- pool
2. +Lactose
3. +Gallic Acid
B
Cluster Area
C-epitope
N-epitope
D
Avg Cell Surface Area (a.u.)
F
RhoA
Avg Fluorescence Intensity (a.u.)
G
ROCK1
C
F-actin
+GA
50µm
E
RhoA-ROCK1
H
CAV1-PTRF PLA assay
Scale bar=20µm
J
YAP1
L
Lamin A
DAP1
N
pγH2AX
I
CAV1-PTRF PLA Avg. Fluorescence Intensity (a.u.)
K
M
LAMIN A
O
P
NFATC2
Gal-3C
Gal-3N
+L
R
MEF2A
T
LDHA dot blot
Q
NFACTC2
S
MEF2
U
LDHA
ns

FIGURE 11

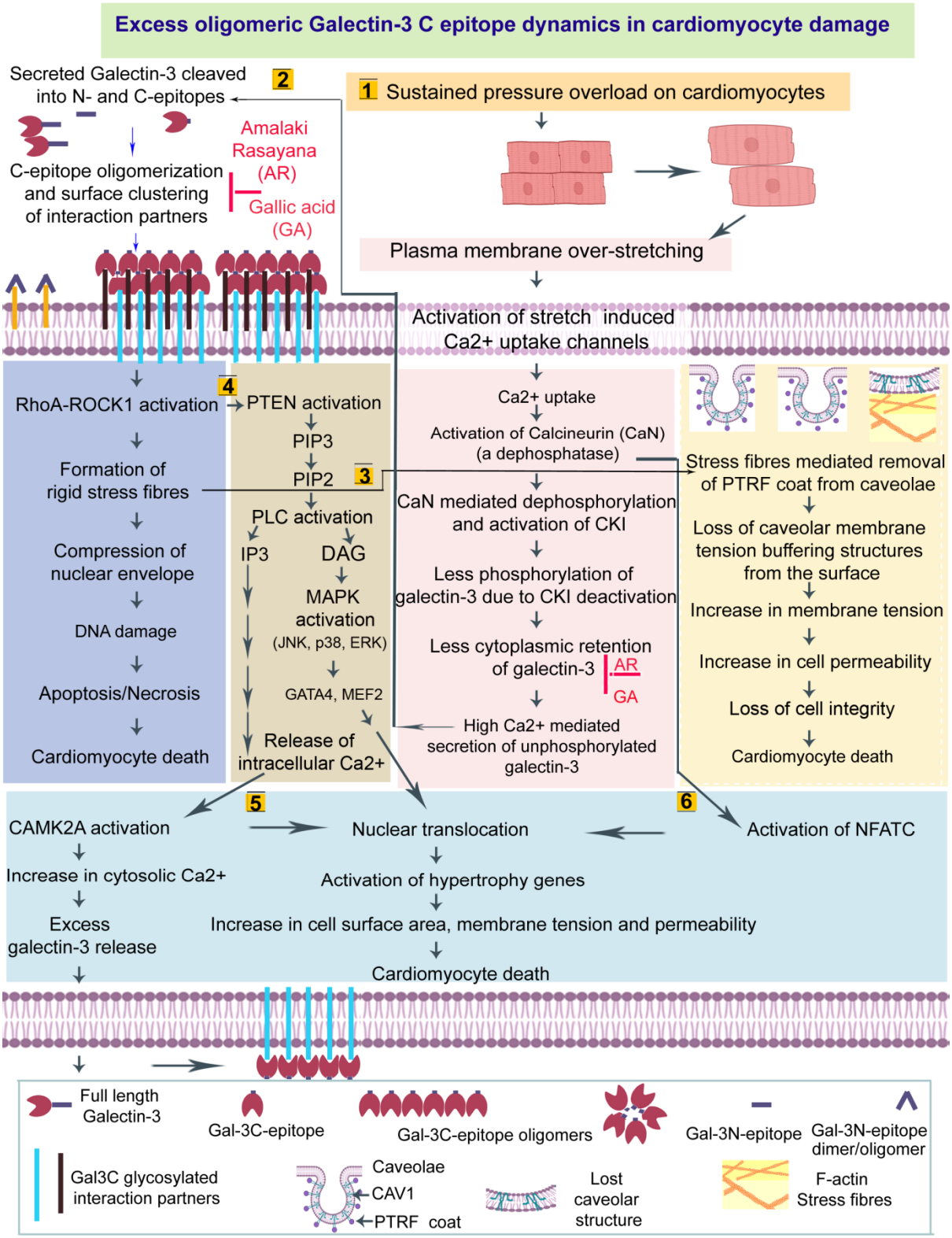
Excess oligomeric Galectin-3 C epitope dynamics in cardiomyocyte damage
Secreted Galectin-3 cleaved into N- and C-epitopes
2
1 Sustained pressure overload on cardiomyocytes
C-epitope oligomerization and surface clustering of interaction partners
Amalaki Rasayana (AR)
Gallic acid (GA)
Plasma membrane over-stretching
Activation of stretch induced Ca2+ uptake channels
RhoA-ROCK1 activation
4
PTEN activation
PIP3
PIP2
3
Formation of rigid stress fibres
Compression of nuclear envelope
DNA damage
Apoptosis/Necrosis
Cardiomyocyte death
PLC activation
IP3
DAG
MAPK activation (JNK, p38, ERK)
GATA4, MEF2
Release of intracellular Ca2+
Ca2+ uptake
Activation of Calcineurin (CaN) (a dephosphatase)
CaN mediated dephosphorylation and activation of CKI
Less phosphorylation of galectin-3 due to CKI deactivation
Less cytoplasmic retention of galectin-3
AR
GA
High Ca2+ mediated secretion of unphosphorylated galectin-3
Stress fibres mediated removal of PTRF coat from caveolae
Loss of caveolar membrane tension buffering structures from the surface
Increase in membrane tension
Increase in cell permeability
Loss of cell integrity
Cardiomyocyte death
5
6
CAMK2A activation
Increase in cytosolic Ca2+
Excess galectin-3 release
Nuclear translocation
Activation of hypertrophy genes
Increase in cell surface area, membrane tension and permeability
Cardiomyocyte death
Activation of NFATC
Full length Galectin-3
Gal-3C-epitope
Gal-3C-epitope oligomers
Gal-3N-epitope
Gal-3N-epitope dimer/oligomer
Gal3C glycosylated interaction partners
Caveolae
CAV1
PTRF coat
Lost caveolar structure
F-actin Stress fibres

FIGURE 12

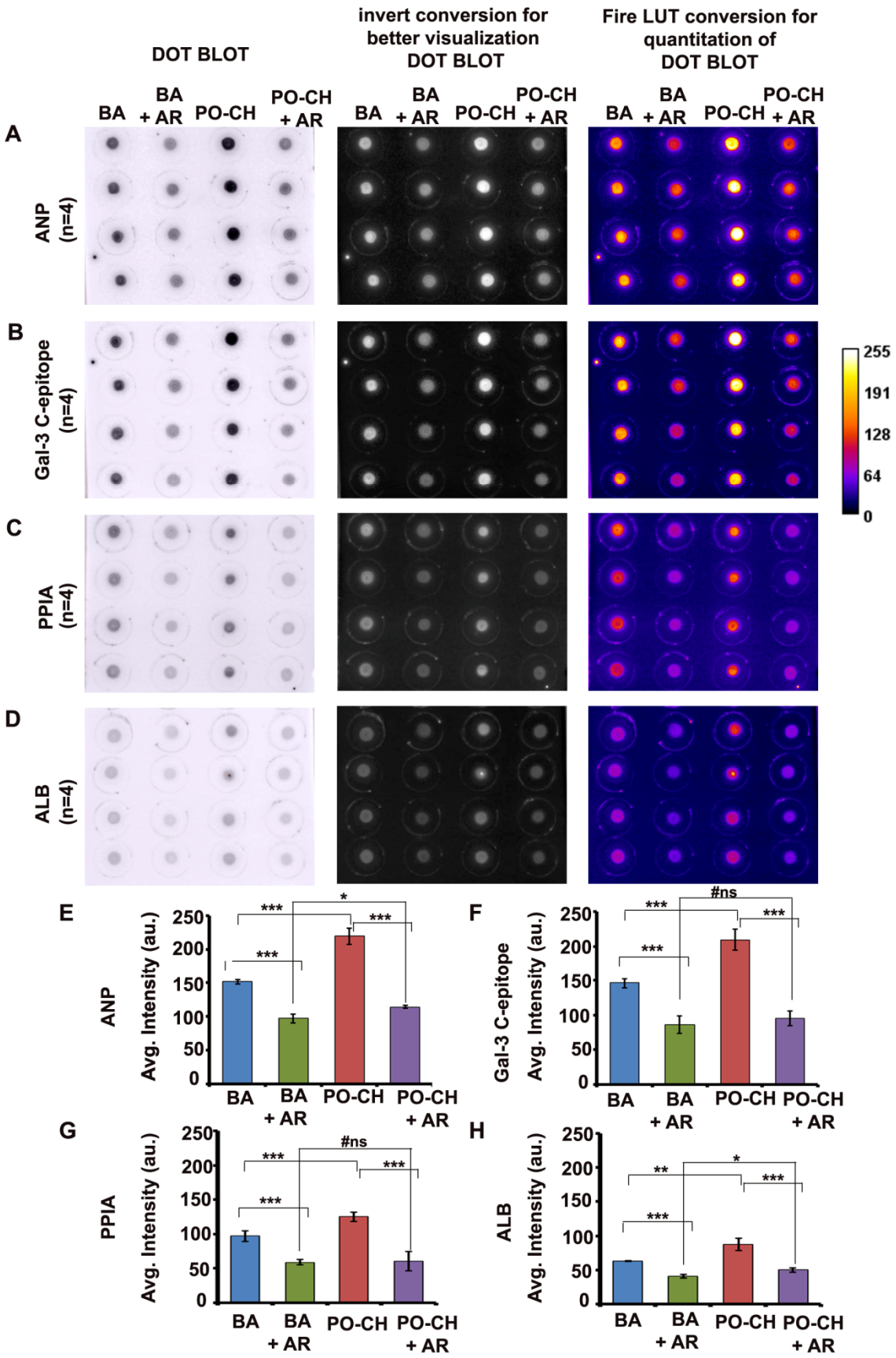
DOT BLOT
invert conversion for better visualization DOT BLOT
Fire LUT conversion for quantitation of DOT BLOT
BA
BA + AR
PO-CH
PO-CH + AR
A
ANP (n=4)
B
Gal-3 C-epitope (n=4)
C
PPIA (n=4)
D
ALB (n=4)
255
191
128
64
0
E
F
G
H
Avg. Intensity (au.)
250
200
150
100
50
0
***
**
*
#ns

FIGURE 13

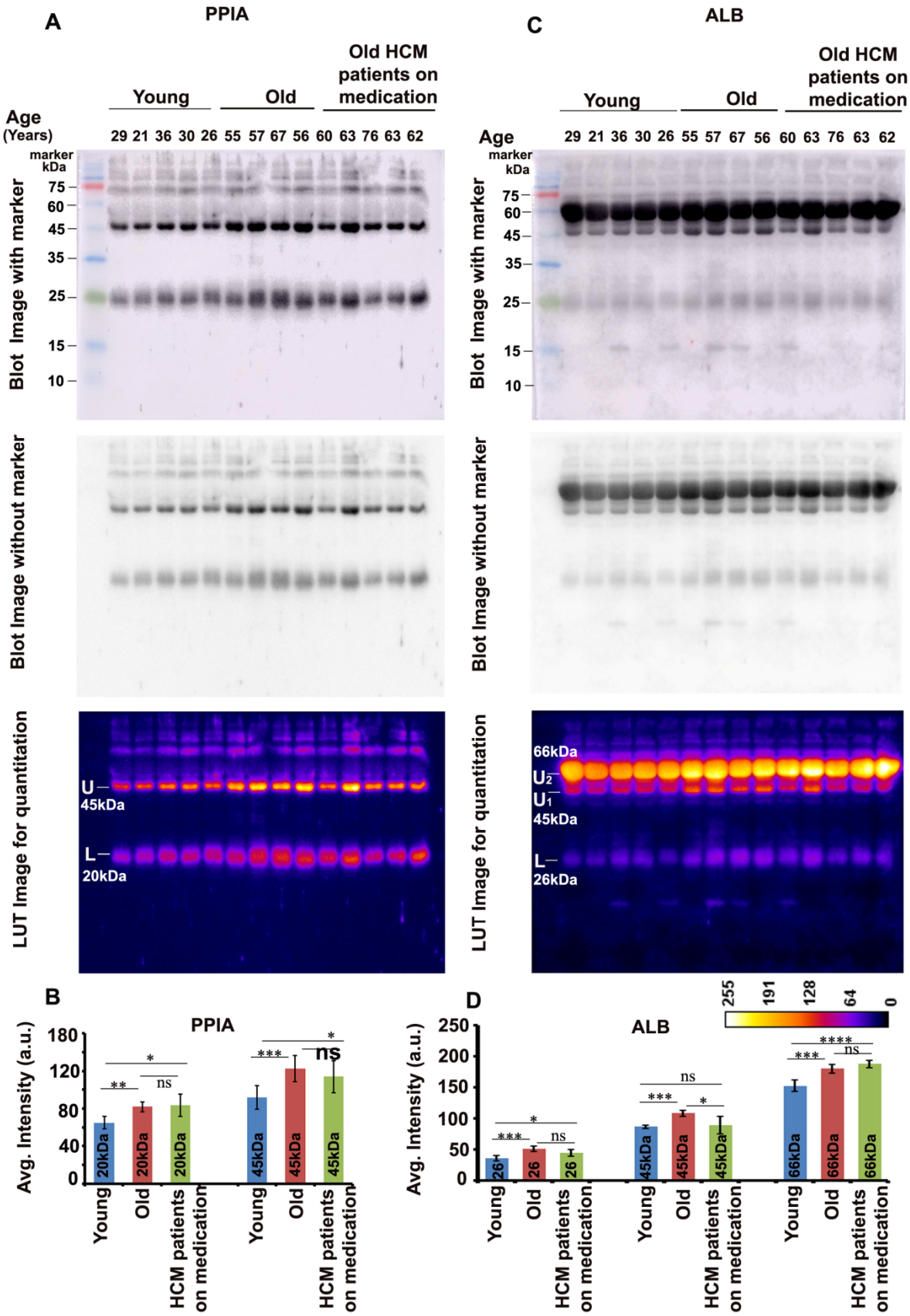
A
PPIA
Young
Old
Old HCM patients on medication
Age (Years)
29 21 36 30 26 55 57 67 56 60 63 76 63 62
marker kDa
75
60
45
35
25
15
10
Blot Image with marker
Blot Image without marker
LUT Image for quantitation
U
45kDa
L
20kDa
C
ALB
Young
Old
Old HCM patients on medication
Age
29 21 36 30 26 55 57 67 56 60 63 76 63 62
marker kDa
75
60
45
35
25
15
10
Blot Image with marker
Blot Image without marker
LUT Image for quantitation
66kDa
U2
U1
45kDa
L
26kDa
B
PPIA
Avg. Intensity (a.u.)
180
120
80
40
0
20kDa
45kDa
Young
Old
HCM patients on medication
D
ALB
Avg. Intensity (a.u.)
250
200
150
100
50
0
26
45kDa
66kDa
255
191
128
64
0
ns
*
**
***
****

FIGURE 14

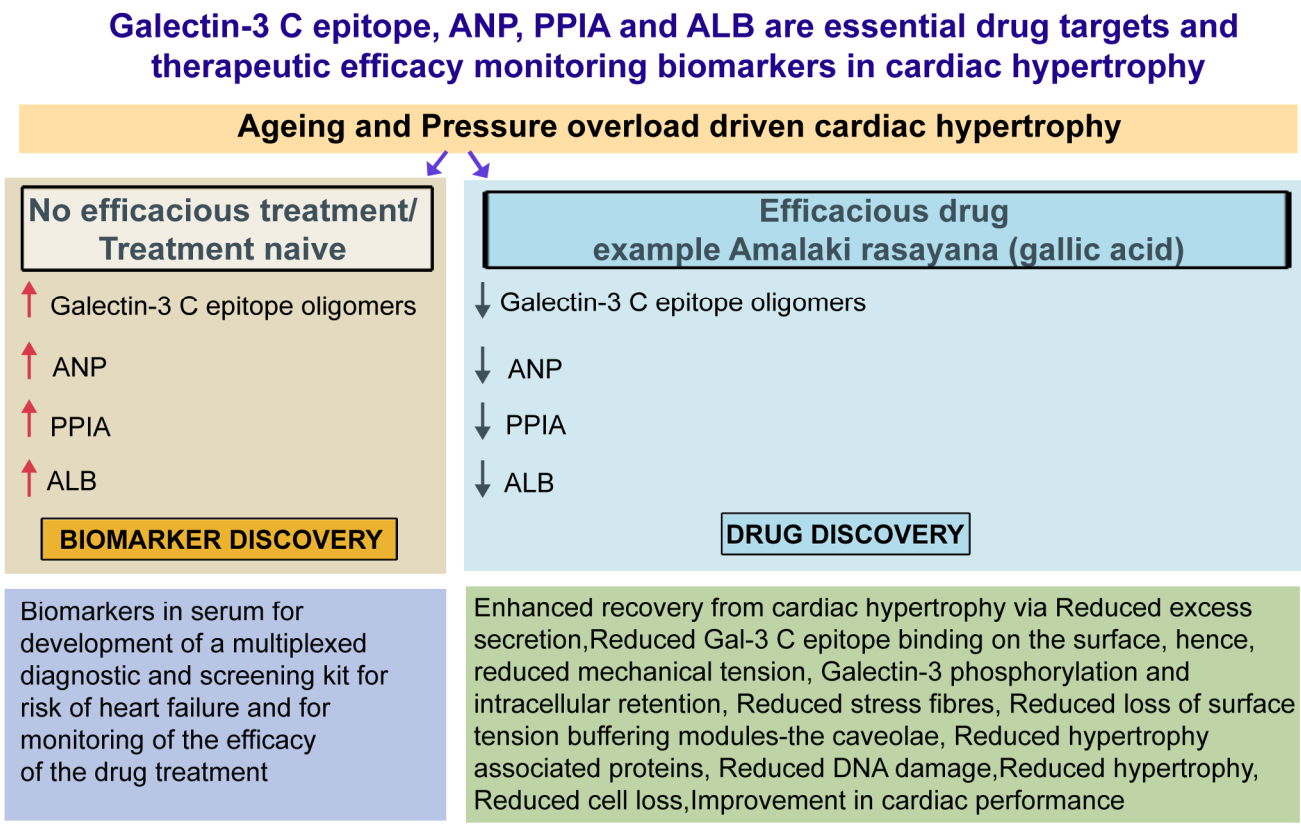
Galectin-3 C epitope, ANP, PPIA and ALB are essential drug targets and therapeutic efficacy monitoring biomarkers in cardiac hypertrophy
Ageing and Pressure overload driven cardiac hypertrophy
No efficacious treatment/ Treatment naive
Galectin-3 C epitope oligomers
ANP
PPIA
ALB
BIOMARKER DISCOVERY
Efficacious drug example Amalaki rasayana (gallic acid)
Galectin-3 C epitope oligomers
ANP
PPIA
ALB
DRUG DISCOVERY
Biomarkers in serum for development of a multiplexed diagnostic and screening kit for risk of heart failure and for monitoring of the efficacy of the drug treatment
Enhanced recovery from cardiac hypertrophy via Reduced excess secretion,Reduced Gal-3 C epitope binding on the surface, hence, reduced mechanical tension, Galectin-3 phosphorylation and intracellular retention, Reduced stress fibres, Reduced loss of surface tension buffering modules-the caveolae, Reduced hypertrophy associated proteins, Reduced DNA damage,Reduced hypertrophy, Reduced cell loss,Improvement in cardiac performance

FIGURE 15